Available online at www.sciencedirect.com
SCIENCE DIRECT®
Neuroscience Letters 395 (2006) 18–22
Neuroscience Letters
www.elsevier.com/locate/neulet

# Cochlear damage due to germanium-induced mitochondrial dysfunction in guinea pigs

Tatsuya Yamasoba [a,*], Yu-ichi Goto [b], Hirofumi Komaki [b], Masakazu Mimaki [b], Akira Sudo [b], Mitsuya Suzuki [a]

[a] *Department of Otolaryngology, Head and Neck Surgery, University of Tokyo, Hongo 7-3-1, Bunkyo-ku, Tokyo 113-8655, Japan*
[b] *Department of Mental Retardation and Birth Defect Research, National Institute of Neuroscience, National Center of Neurology and Psychiatry, Tokyo, Japan*

Received 24 August 2005; received in revised form 17 October 2005; accepted 17 October 2005

**Abstract**

This investigation addressed the effect of germanium dioxide ($GeO_2$)-induced mitochondrial dysfunction on hearing acuity. Guinea pigs were fed chow that contained 0%, 0.15%, or 0.5% $GeO_2$. The animals that were fed 0.5% $GeO_2$ for 2 months developed hearing impairment chiefly due to degeneration of stria vascularis and cochlear supporting cells, which exhibited electron-dense mitochondrial inclusions. Cytochrome *c* oxidase activity was decreased in the skeletal muscles and kidney, which also exhibited electron-dense mitochondrial inclusions. No apparent pathological changes were observed in the utricle, semicircular canal, or among the vestibular nerve fibers, or in the liver or heart. The untreated animals and those treated with 0.15% $GeO_2$ did not exhibit hearing impairment or pathological changes in any organs. These findings suggest that administration of 0.5% $GeO_2$ induces mitochondrial dysfunction in the stria vascularis and supporting cells in the cochlea, as in the skeletal muscles and kidney, thereby causing hearing impairment in the guinea pigs.


*Keywords:* Hearing loss; Mitochondrial myopathy; Mitochondrial DNA; Cochlea; Muscle; Kidney

Mutations in mitochondrial DNA (mtDNA) are reported to be closely associated with both syndromic and nonsyndromic forms of sensorineural hearing loss (SNHL) [14]. SNHL occurs in approximately 70% of the three most common mitochondrial disorders: mitochondrial myopathy, encephalopathy, lactic acidosis and stroke-like episodes (MELAS), myoclonus epilepsy associated with ragged-red fiber, and chronic progressive external ophthalmoplegia (CPEO) [14]. SNHL is also frequently manifested in subjects with other mtDNA mutations, particularly those in 12S rRNA and $tRNA^{Ser(UCN)}$ [2]. In general, SNHL due to mtDNA lesions primarily involves the cochlea, while the vestibular system and retrocochlear auditory pathway are well preserved [1,11,17]. The fact that mtDNA lesions frequently cause SNHL of cochlear origin suggests that certain sets of cochlear cells have a high metabolic demand and are strongly dependent upon mitochondrial function. Human temporal bone histopathology has been reported only in four patients with SNHL associated with mtDNA lesions [7,13,20], in which the stria vascularis (SV) exhibited degeneration but other cochlear tissues such as hair cells were not always affected. It is therefore unclear which cochlear cells are preferentially affected by chronic mitochondrial dysfunction associated with mtDNA lesions.

There are several animal models, including genetically modified mice, that exhibit certain forms of mitochondrial dysfunction [15]. Auditory function has been studied in mice with mutant mtDNA carrying a 4696-base pair deletion, which develop hearing loss when the heteroplasmy is greater than 80% [8]. To date, cochlear histopathology has not been studied in these mice. Other animal models can be created by introducing harmful agents into the mitochondria. Hoya et al. [5] applied a mitochondrial toxin, 3-nitropropionic acid (3-NP), topically to rat cochlea and found that animals treated with 500 mM of 3-NP exhibited permanent threshold shifts. Histologically, there was degeneration of fibrocytes in the spiral ligament and spiral limbus, which indicated that these tissues may be vulnerable to acute mitochondrial dysfunction. Another animal model was created by chronic application of germanium

* Corresponding author. Tel.: +81 3 5800 8924; fax: +81 3 3814 9486.
*E-mail address:* tyamasoba-tky@umin.ac.jp (T. Yamasoba).

0304-3940/$ – see front matter © 2005 Elsevier Ireland Ltd. All rights reserved.
doi:10.1016/j.neulet.2005.10.045

dioxide ($GeO_2$). This model is of special interest since in humans, long-term administration of high doses of $GeO_2$ causes renal failure, emaciation, and muscle weakness [3,10]. Germanium compounds are readily absorbed following oral exposure, distributed throughout the body tissues, particularly the kidney and thyroid, and excreted largely in the urine. Rats that are fed chow containing $GeO_2$ exhibit body weight loss, myopathy, and nephropathy, and their skeletal muscles show numerous ragged-red fibers, cytochrome *c* oxidase (COX)-deficient fibers, and accumulation of electron-dense material in the mitochondria [3,4,9,16]. These pathological findings resemble those observed in patients with mitochondrial encephalomyopathy. Although the precise mechanism of toxicity of $GeO_2$ is unknown, recent study demonstrated that rats treated with $GeO_2$ for 24 weeks showed increased free radical generation and decreased mitochondrial DNA copies in the skeletal muscles compared to controls given normal diet [6]. Thus, chronic administration of $GeO_2$ may provide a controlled model for assessment of mitochondrial dysfunction-induced SNHL and allow analysis of the specific histopathology underlying this clinically significant disorder.

Thirty-six albino male guinea pigs (250–300 g, approximately 4 weeks after birth) with auditory brainstem response (ABR) thresholds within the normal laboratory range were used. Twelve animals were assigned to one of the three groups and fed standard guinea pig chow containing 0% (control), 0.15%, or 0.5% $GeO_2$. The controls and animals that were administered 0.15% $GeO_2$ were allowed to survive for 6 months, but animals administered 0.5% $GeO_2$ were sacrificed after 2 months because many became inactive and appeared less healthy at that time. Animals were caged singularly in an ambient room under a 12-h light:12-h dark cycle beginning at 06:00 h. Food and water were available ad libitum. Clinical manifestations and the body weight of each animal were observed every 2 weeks. Pure-tone ABRs were measured every 4 weeks. The experimental protocol was approved by the Committee for the Use and Care of Animals at the University of Tokyo and conformed to the NIH Guidelines for the Care and Use of Laboratory Animals.

The method for ABR measurement has been previously described [19]. In brief, the animals were anesthetized with xylazine hydrochloride (10 mg/kg, i.m.) and ketamine hydrochloride (40 mg/kg, i.m.). Following anesthetization, needle electrodes were placed subcutaneously at the vertex (active electrode), beneath the pinna of the left ear (reference electrode), and beneath the right ear (ground). The sound stimulus consisted of a 15-ms tone burst, with a rise-fall time of 1 ms at frequencies of 2, 4, 8, and 16 kHz. The responses of 1024 sweeps were averaged at each intensity level (5 dB steps) to assess the threshold. Hearing threshold was defined as the lowest stimulus intensity that produced a reliable peak 3 or 4 in ABR waveforms. The effect of $GeO_2$ on the ABR thresholds was analyzed by comparing the final thresholds, measured 2 month later for animals that were administered 0.5% $GeO_2$ and 6 month later for those given 0.15% $GeO_2$ and controls, among the three groups using one-way ANOVA followed by a multiple comparison procedure (Student–Newman–Keuls method).

The controls and animals that were administered 0.15% $GeO_2$ were sacrificed 6 months later. The animals that were administered 0.5% $GeO_2$ were sacrificed after 2 months because most of them became very inactive and seemingly unhealthy at that time. Under anesthesia with xylazine hydrochloride (10 mg/kg, i.m.) and ketamine hydrochloride (40 mg/kg, i.m.), the bulla in the left ear was exposed, a small opening was made in the scala tympani, and the perilymphatic spaces were perfused with a fixative containing 2% paraformaldehyde and 2.5% glutaraldehyde in phosphate buffer. This was followed by immediate excision of the soleus and extensor digitorum longus (EDL) muscles, liver, kidney, and heart. A part of these organs was quickly frozen in isopentane chilled in liquid nitrogen, and the remaining specimens were immersed in the fixative. The left temporal bone was then excised, immersed in the same fixative, decalcified in 10% ethylenediaminetetraacetic acid, and divided into cochlear and vestibular parts. The cochlea was incised parallel to the modiolus and the utricular macula and ampulla of the lateral semicircular canal were obtained. For electron microscopy, all the fixed specimens (muscle, liver, kidney, heart, cochlea, utricle, and lateral semicircular canal) were post-fixed in 1% osmium tetroxide, dehydrated in a graded ethanol series, and embedded in epoxy resin. Ultrathin sections were double stained with uranyl acetate and lead citrate and examined with a transmission electron microscope (TEM), as previously described [18]. Serial frozen sections of the skeletal muscle, heart, kidney, and liver were also stained with hematoxylin and eosin (H&E) and an antibody to COX, as previously described [16].

In the controls and animals that were administered 0.15% $GeO_2$, the body weight increased gradually from 280 to 780 g during a period of 6 months. In contrast to this, the weight of animals that were administered 0.5% $GeO_2$ increased slightly to 310 g in the first month and reduced to 295 g in the second month (Fig. 1). The weight loss was accompanied by muscle weakness and atrophy, but none of the animals exhibited apparent neurological abnormalities such as ataxia or convulsions.

The controls and animals that were administered 0.15% $GeO_2$ did not demonstrate shifts in the ABR threshold compared with their baseline values at any frequency during the experiment, whereas the animals that were administered 0.5% $GeO_2$ exhibited significant increase ($p < 0.01$) in the ABR thresholds at all frequencies 2 months later (Fig. 1).

The most prominent findings in the animals that were administered 0.5% $GeO_2$ were marked degeneration of the SV and supporting cells in the organ of Corti (Fig. 2). Vacuolar degeneration, accompanied by abnormal mitochondria containing electron-dense inclusions, was predominantly observed in the SV of the basal turns of the cochlea. Electron-dense mitochondrial inclusions were also observed in the Hensen cells, Boettcher cells, and Claudius cells, all of which showed marked degenerative changes. The inner and outer hair cells (IHCs and OHCs, respectively), pillar cells, and Deiters cells, as well as the basilar and tectorial membranes, showed no obvious signs of pathology. A small amount of electron-dense material was observed along the intact cochlear nerve fibers. No electron-dense material or pathological changes were observed in the utricle, lateral semicircular canal, or among the vestibular nerve

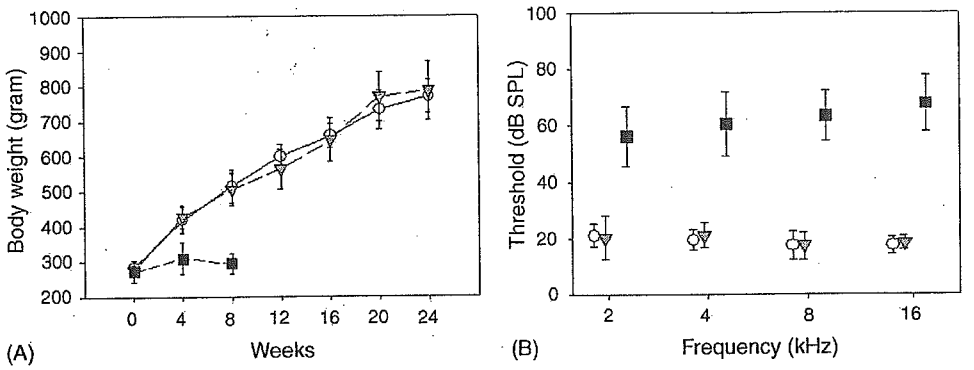


Fig. 1. (A) Change (mean ± S.D.) in whole body weight. (B) Auditory brainstem response thresholds (mean ± S.D.) measured before euthanasia, i.e., 6 months after the initiation of the experiment in controls (○) and animals that were administered 0.15% $GeO_2$ (▽) and 2 months after the initiation in those that were administered 0.5% $GeO_2$ (■).

fibers. In the controls and animals that were administered 0.15% $GeO_2$, no pathological changes or electron-dense material were observed in the cochlea or vestibular endorgans or among the cochlear or vestibular nerve fibers (data not shown).

In the animals that were administered 0.5% $GeO_2$, marked pathological and histochemical changes were observed in the skeletal muscles and kidney. The EDL and soleus muscles, which contained many abnormal mitochondria including electron-dense material, showed marked reduction in COX activity when compared with that of the controls (Fig. 3). Similarly, the kidney exhibited vacuolar degeneration and many electron-dense deposits in the distal tubular epithelium and reduction in COX activity. No apparent morphological or histochemical abnormalities were found in the liver or heart, although a small amount of electron-dense inclusions were observed in the mitochondria of the heart. The controls and animals that were administered 0.15% $GeO_2$ did not show any evidence of pathological changes in any tissue examined. COX activity did not differ in any organs between these groups (data not shown).

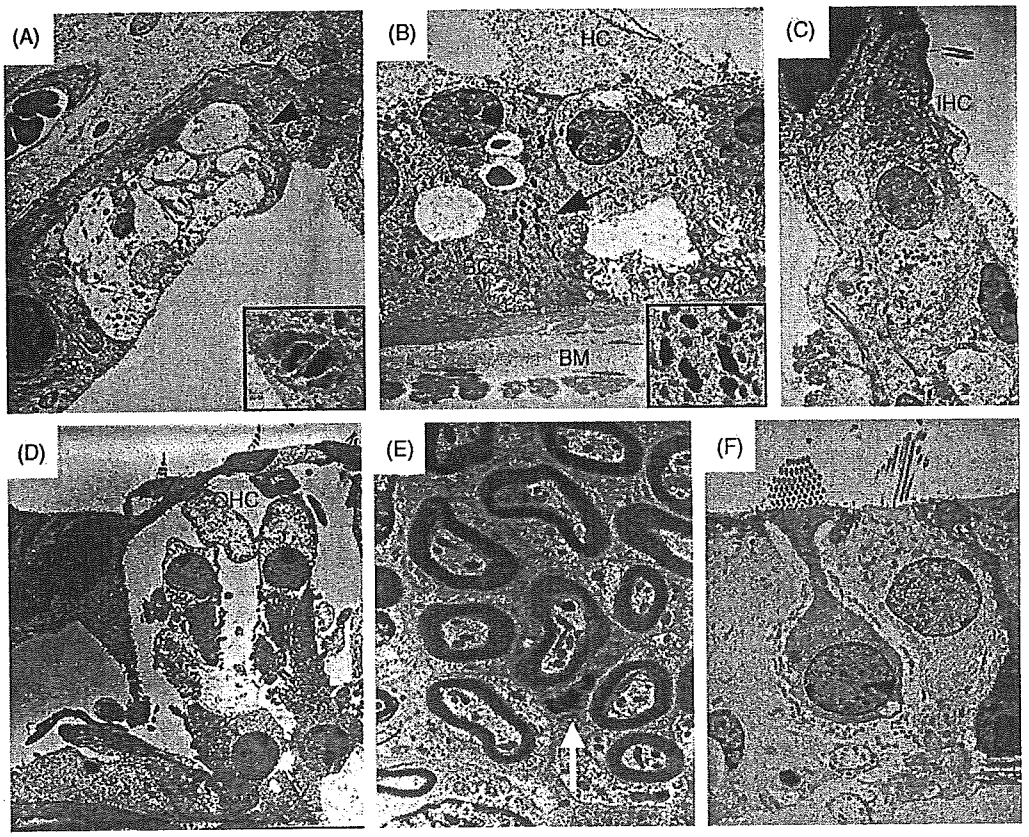


Fig. 2. Ultrastructural findings of the inner ear in animals that were administered 0.5% $GeO_2$. (A) Marked vacuolar degeneration in the stria vascularis (SV). The arrowhead indicates mitochondria containing electron-dense inclusions (inset: high-power view). (B) The supporting cells, such as Hensen cells (HC) and Boettcher cells (BC), in the organ of Corti show marked degenerative changes. The arrowhead indicates the mitochondria containing electron-dense materials (inset: high-power view); BM: basilar membrane. (C) Relatively well preserved inner hair cell (IHC). (D) Relatively well preserved outer hair cells (OHC) and pillar cells (PC). (E) A small amount of mitochondria containing electron-dense materials (white arrow) along the intact cochlear nerve fibers. (F) Normal sensory epithelium of the utricle.

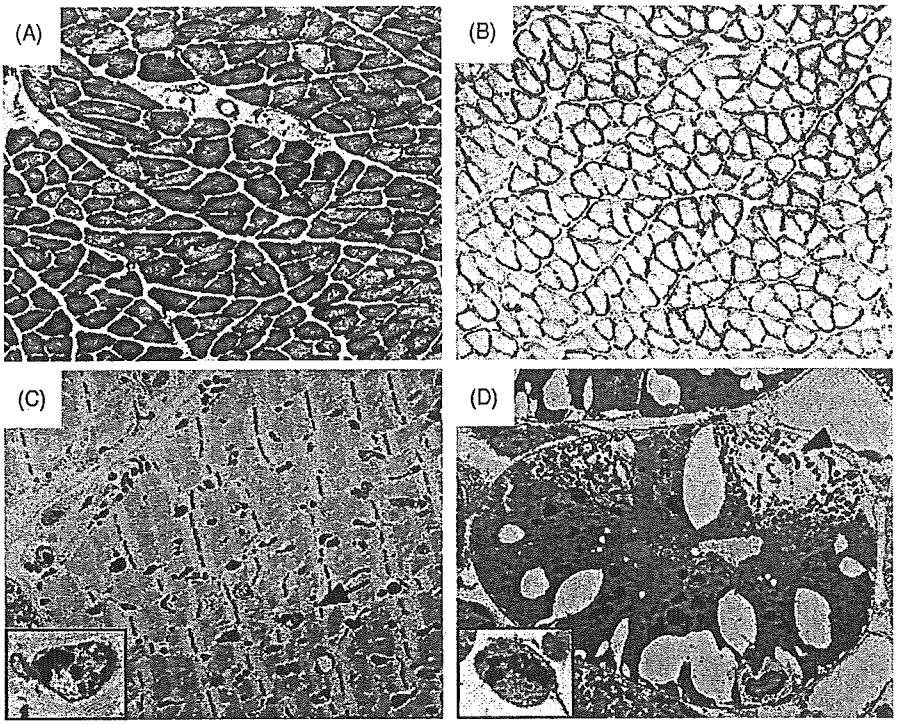


Fig. 3. Frozen sections of the soleus muscle stained with COX from a control (A) and an animal that was administered 0.5% $GeO_2$ (B), showing marked reduction in COX activity in the latter. Ultrastructural findings in extensor digitorum longus muscle (C) and kidney (D) from an animal that was administered 0.5% $GeO_2$. The arrow indicates the muscle showing many degenerated mitochondria containing electron-dense materials (inset: high-power view). The arrowhead indicates the distal tubular epithelium in kidney showing vacuolar degeneration and many electron-dense deposits (inset: high-power view).

The current study showed that chronic administration of 0.5% $GeO_2$, and not 0.15% $GeO_2$, in guinea pigs caused degeneration of the skeletal muscles and kidney, which was associated with electron-dense materials in the mitochondria and the reduction in COX activity. The animals that were administered 0.5% $GeO_2$ also developed severe hearing loss chiefly due to the degeneration of SV and cochlear supporting cells, both of which contained a large amount of electron-dense materials in the mitochondria. These findings suggest that SV and the supporting cells in the cochlea are most preferentially affected by chronic mitochondrial dysfunction in guinea pigs.

While the controls and animals that were administered 0.15% $GeO_2$ showed gradual increase in the body weight from 280 to 780 g during a period of 6 months, the weight of animals that were administered 0.5% $GeO_2$ increased only slightly in the first month and reduced in the second month, which is considered to primarily reflect the loss of muscle mass due to $GeO_2$-induced mitochondrial damage. It is also possible that animals that were administered 0.5% $GeO_2$ ate less than those in the other groups, and may not have consumed on the average 3 1/3 times the amount of $GeO_2$ consumed by the animals administered 0.15% $GeO_2$ in that same period.

The pathological changes in the skeletal muscles and kidney of guinea pigs that were administered 0.5% $GeO_2$ were very similar to those observed in rats that were administered 0.15% $GeO_2$ and human subjects who were administered high doses of $GeO_2$ for a long period of time [3,4,9,10,16]. In a preliminary study, we found that mice that were administered 0.15% $GeO_2$ also developed body weight loss, degeneration of the skeletal muscles and kidney containing electron-dense materials in the mitochondria, and severe hearing loss (Yamada et al., unpublished data). These findings suggest that chronic mitochondrial dysfunction unexceptionally causes the above-mentioned pathologies in mammals, although the $GeO_2$ concentration that causes mitochondrial dysfunction may differ among species.

Human temporal bone histopathological findings associated with mtDNA lesions have been reported in four patients. In a patient with MELAS and moderate SNHL, marked SV atrophy, partial loss of the IHCs and OHCs, moderate loss of the spiral ganglion cells (SGCs), and loss of sensory cells in the vestibular endorgans were observed [13]. Another patient with MELAS and moderate SNHL exhibited severe SV atrophy, intact IHCs and OHCs, and only mildly degenerated SGCs [13]. A totally deaf patient with Kearns–Sayre syndrome, a form of CPEO, exhibited marked degeneration of the SV, spiral prominence, and organ of Corti; slight reduction in the number of SGCs; and well preserved semicircular canals and utricle [7]. A totally deaf patient with maternally inherited diabetes and deafness associated with A3243G mutation exhibited marked SV atrophy, partial loss of the OHCs, and loss of the SGCs in the basal turn, whereas the IHCs and vestibular endorgans were well preserved [20]. These findings suggest that in humans, SV is the first to be affected by mitochondrial dysfunction; the organ of Corti including the supporting cells, the second; the SGCs, the third; and vestibular endorgans, the last. This pattern of inner ear cell involvement in human mtDNA lesions is similar to that observed in the guinea pigs that were administered 0.5% $GeO_2$, which is indicative of the fact that animals treated with $GeO_2$

can be used to study the mechanism of hearing impairment and cochlear damage associated with mtDNA lesions.

Many previous animal studies that investigated noise-induced or aminoglycoside-induced damage have shown that the OHCs are more vulnerable to these stresses compared to the IHCs and supporting cells [12,19]. In contrast, in the current study, the supporting cells were damaged while the IHCs and OHCs remained nearly intact. $GeO_2$ may have been distributed more preferentially to the supporting cells, resulting in their preferential degeneration. Alternatively, the supporting cells may be more susceptible to mitochondrial dysfunction than the hair cells. In either case, the histological findings suggest that we need to check more carefully the status of supporting cells of the organ of Corti in studies of stress induced damage.

In conclusion, the current study suggests that chronic mitochondrial dysfunction may most preferentially affect the SV and supporting cells in the guinea pig cochlea. This animal model is considered useful for studying the SNHL mechanism associated with mtDNA lesions. The next step is to determine the genes that are involved in SNHL development in this animal model, which provides invaluable information on the prevention/retardation of SNHL in patients harboring mtDNA lesions. It may also be worthwhile to examine if the manifestation of phenotype in this animal model can be prevented or retarded by calorie restriction, which causes a metabolic shift toward increased protein turnover and decreased macromolecular damage, and by supplements, such as alpha lipoic acid and acetyl-L-carnitine, that have a capacity to enhance mitochondrial bioenergetics.

## Acknowledgments

This work was supported by grants from the Ministry of Health, Labour and Welfare and the Ministry of Education, Culture, Sports, Science and Technology in Japan to Tatsuya Yamasoba. We thank Mr. Y. Mori for providing us with technical assistance.

## References

[1] P.F. Chinnery, C. Elliot, G.R. Green, A. Rees, A. Coulthard, D.M. Turnbull, T.D. Griffiths, The spectrum of hearing loss due to mitochondrial DNA defects, Brain 123 (2000) 82–92.
[2] N. Fischel-Ghodsian, Mitochondrial deafness, Ear Hear 24 (2003) 303–313.
[3] I. Higuchi, S. Izumo, M. Kuriyama, M. Suehara, M. Nakagawa, H. Fukunaga, M. Osame, S. Ohtsubo, K. Miyata, Germanium myopathy: clinical and experimental pathological studies, Acta Neuropathol. (Berl.) 79 (1989) 300–304.
[4] I. Higuchi, K. Takahashi, K. Nakahara, E. Izumo, M. Nakagawa, M. Osame, Experimental germanium myopathy, Acta Neuropathol. (Berl.) 82 (1991) 55–59.
[5] N. Hoya, Y. Okamoto, K. Kamiya, M. Fujii, T. Matsunaga, A novel animal model of acute cochlear mitochondrial dysfunction, NeuroReport 15 (2004) 1597–1600.
[6] X. Li, F. Gao, Q. Chen, The pathogenesis of experimental model of mitochondrial myopathy induced by germanium dioxide, Chin. Med. Sci. J. 16 (2001) 157–160.
[7] J.R. Lindsay, R. Hinojosa, Histopathologic features of the inner ear associated with Kearns–Sayre syndrome, Arch. Otolaryngol. 102 (1976) 747–752.
[8] K. Nakada, A. Sato, H. Sone, A. Kasahara, K. Ikeda, Y. Kagawa, H. Yonekawa, J. Hayashi, Accumulation of pathogenic DeltamtDNA induced deafness but not diabetic phenotypes in mito-mice, Biochem. Biophys. Res. Commun. 323 (2004) 175–184.
[9] T. Sanai, N. Oochi, S. Okuda, S. Osato, S. Kiyama, T. Komota, K. Iseki, M. Fujishima, Subacute nephrotoxicity of germanium dioxide in the experimental animal, Toxicol. Appl. Pharmacol. 103 (1990) 345–353.
[10] T. Sanai, S. Okuda, K. Onoyama, N. Oochi, Y. Oh, K. Kobayashi, K. Shimamatsu, S. Fujii, M. Fukushima, Germanium dioxide-induced nephropathy: a new type of renal disease, Nephron 54 (1990) 53–60.
[11] C.M. Sue, L.J. Lipsett, D.S. Crimmins, C.S. Tsang, S.C. Boyages, C.M. Presgrave, W.P. Gibson, E. Byrne, J.G. Morris, Cochlear origin of hearing loss in MELAS syndrome, Ann. Neurol. 43 (1998) 350–359.
[12] M. Sugawara, G. Corfas, M.C. Liberman, Influence of supporting cells on neuronal degeneration after hair cell loss, J. Assoc. Res. Otolaryngol. 6 (2005) 136–147.
[13] K. Takahashi, S.N. Merchant, T. Miyazawa, T. Yamaguchi, M.J. McKenna, H. Kouda, Y. Iino, T. Someya, Y. Tamagawa, Y. Takiyama, I. Nakano, K. Saito, P. Boyer, K. Kitamura, Temporal bone histopathological and quantitative analysis of mitochondrial DNA in MELAS, Laryngoscope 113 (2003) 1362–1368.
[14] D.C. Wallace, Diseases of mitochondrial DNA, Ann. Rev. Biochem. 61 (1992) 1175–1212.
[15] D.C. Wallace, Mouse models for mitochondrial disease, Am. J. Med. Genet. 106 (2001) 71–93.
[16] C.M. Wu, T. Matsuoka, M. Takemitsu, Y. Goto, I. Nonaka, An experimental model of mitochondrial myopathy: germanium-induced myopathy and coenzyme Q10 administration, Muscle Nerve 15 (1992) 1258–1264.
[17] T. Yamasoba, Y. Oka, K. Tsukuda, M. Nakamura, K. Kaga, Auditory findings in patients with maternally inherited diabetes and deafness harboring a point mutation in the mitochondrial transfer $RNA^{Leu(UUR)}$ gene, Laryngoscope 106 (1996) 49–53.
[18] T. Yamasoba, M. Suzuki, K. Kaga, Influence of chronic kanamycin administration on basement membrane anionic sites in the labyrinth, Hear Res. 102 (1996) 116–124.
[19] T. Yamasoba, J. Schacht, F. Shoji, J.M. Miller, Attenuation of cochlear damage from noise trauma by an iron chelator, a free radical scavenger and glial cell line-derived neurotrophic factor in vivo, Brain Res. 815 (1999) 317–325.
[20] T. Yamasoba, K. Tsukuda, Y. Oka, T. Kobayashi, K. Kaga, Cochlear pathology associated with mitochondrial $tRNA^{Leu(UUR)}$ gene mutation, Neurolog1 52 (1999) 1705–1707.

Cell Tissue Res
DOI 10.1007/s00441-006-0157-9



REGULAR ARTICLE

Tatsuya Yamasoba · Kenji Kondo

# Supporting cell proliferation after hair cell injury in mature guinea pig cochlea in vivo

Received: 4 October 2005 / Accepted: 4 January 2006


**Abstract** In cold-blooded animals, lost sensory hair cells can be replaced via a process of regenerative cell proliferation of epithelial supporting cells. In contrast, in mammalian cochlea, receptor (hair) cells are believed to be produced only during embryogenesis; after maturity, sensory or supporting cell proliferation or regeneration are thought to occur neither under normal conditions nor after trauma. Using bromodeoxyuridine (BrdU) as a proliferation marker, we have assessed cell proliferation activity in the mature organ of Corti in the cochlea of young guinea pigs following severe damage to the outer hair cells induced by kanamycin sulfate and ethacrynic acid. Although limited, we have found BrdU-labeled nuclei in the regions of Deiters cells when BrdU is given for 3 days or longer. When BrdU is given for 10 days, at least one labeled nucleus can be observed in the organ of Corti in approximately half of the ears; proliferating cells typically appear as paired daughters, with one nucleus being displaced away from the basement membrane to the position expected of the hair cells. Double-staining with antibodies to cytokeratin, vimentin, and p27 have shown that the BrdU-labeled nuclei are located in cells phenotypically similar to Deiters cells. Most of the uptake of BrdU occurs 3–5 days following ototoxic insult, and the number of BrdU-labeled cells does not decrease until 30 days following insult. These findings indicate that Deiters cells in the mature mammalian cochlea maintain a limited competence to re-enter the cell cycle and proliferate after hair cell injury, and that they can survive at least for 1 month.

**Keywords** Cochlea · BrdU · p27 · Deiters cell · Hair cell · Regeneration · Guinea pig

## Introduction

Sensory receptors (hair cells) in the mammalian ear are located in the cochlear organ of Corti (OC) and in the vestibular sensory epithelia of the saccular macula, the utricular macula, and the cristae of the three semicircular canals. Two types of hair cells have been found in the OC: the inner (IHCs) and outer (OHCs) hair cells. The human cochlea possesses approximately 3,500 IHCs and approximately 12,000 OHCs. The IHCs are arranged in a single row and receive approximately 95% of their afferent innervation from the acoustic nerve. The OHCs are mostly arranged in three rows and contain a motile protein that induces contraction with stimulation and finely tune the response of the basilar membrane in order to determine the sharpness of the traveling wave generated by sound stimulation (Slepecky 1996). Hair cells in the mammalian OC are believed to be formed during a limited period of embryonic development, and after maturity, they are not thought to be replaced when they die (Ruben 1967; Bermingham-McDonogh and Rubel 2003). In humans, auditory hair cells can be damaged and lost as a consequence of acoustic trauma, treatment with ototoxic agents, infections, autoimmune pathologies, genetic susceptibilities, or as a part of the aging process. The loss of auditory hair cells in the human cochlea is a leading cause of permanent hearing deficits, currently affecting an estimated 600 million worldwide.

Lineage studies have shown that sensory hair cells and supporting cells arise from common progenitors in the inner ear (Lang and Fekete 2001). In cold-blooded animals, lost sensory hair cells can be quickly replaced via a process of regenerative cell proliferation of epithelial supporting

This work was supported by the Ministry of Health, Labour, and Welfare, Japan (grants 12120101, 15110201) and by the Ministry of Education, Culture, Sports, Science, and Technology, Japan (grant 13470357) to T.Y.

T. Yamasoba (✉) · K. Kondo
Department of Otolaryngology and Head and Neck Surgery,
University of Tokyo,
Hongo 7-3-1, Bunkyo-ku,
Tokyo, 113-8655, Japan
e-mail: tyamasoba-tky@umin.ac.jp
Tel.: +81-3-58008924
Fax: +81-3-38149486

cells, which re-enter the cell cycle after hair cell injury (Corwin and Cotanche 1988; Ryals and Rubel 1988; Stone and Cotanche 1994; Bhave et al. 1995; Stone et al. 1999; Stone and Rubel 2000). A more limited regenerative response also has been observed in the damaged vestibular organs of mammals in which the reoccurrence of hair cells also reflects cell proliferation; this is most readily observed after treatment with mitogenic growth factors (Forge et al. 1993; Rubel et al. 1995; Li and Forge 1997; Kuntz and Oesterle 1998). Hair cell proliferation in the mammalian vestibular sensory epithelium encourages the expectation that a similar regeneration via cell proliferation may be possible in the mature mammalian cochlea after hair cell injury. Indeed, one controversial report suggests that in vitro retinoic acid can induce regeneration of auditory hair cells in ototoxic-poisoned rat OC explants (Lefebvre et al. 1993); however, other researchers have failed to confirm this finding (Chardin and Romand 1995). Although intensively sought, no evidence of cell proliferation has been observed to date in the postnatal mammalian OC (Ruben 1967; Roberson and Rubel 1994; Yamasoba et al. 2003; Bermingham-McDonogh and Rubel 2003). In part, this may reflect a limitation in the techniques used in these previous studies, which are largely based on the sectioning of the OC. Thus, labeled cells expressing the used proliferation marker may have been missed in the sectioned cochlea, in which it is impossible to observe all cells in the OC throughout the cochlea. We have therefore applied a surface preparation technique that has allowed us to observe the auditory sensory epithelium throughout the injured cochlea in a search to detect single bromodeoxyuridine (BrdU)-labeled cells.

## Materials and methods

### Animals

We employed 120 young albino guinea pigs (250–350 g) that had normal baseline auditory brainstem response (ABR) thresholds at 4, 8, and 20 kHz within the normal laboratory range.

### Experimental protocol

The first aim of this study was to assess cell proliferation in the OC following hair cell injury. Ten animals that were deafened by systemic administration of kanamycin sulfate (KM) and ethacrynic acid (EA) on day 1 were given BrdU daily for 10 days from day 2 through day 11 and killed on day 12, 12 h following the last BrdU injection. This paradigm was set to exclude the possibility of the detection of dying cells that could passively take up BrdU. The OC was stained with antibodies to BrdU and observed under confocal laser microscopy. Eight control animals that were not deafened but that were given BrdU similarly for 10 days were also killed to investigate whether mitosis occurred in the normal OC ($n$=5) and for negative histological controls ($n$=3). The second aim, if BrdU-labeled cells were found, was to identify the type of cells labeled and to define the time window of their occurrence and the duration of their survival. Forty deafened animals were given BrdU daily for 10 days, from day 2 (following KM+EA) through day 11, and killed on day 12, 12 h following the last BrdU injection. In 10 of these animals, BrdU-labeled cells were made visible by the reaction to diaminobenzidine (DAB), and the surface and lateral views of the OC were examined under Nomarski optics at the light microscope level and by transmission electron microscopy (TEM). The remaining 30 animals were double-stained with antibodies to BrdU and p27 ($n$=10), cytokeratins ($n$=10), or vimentin ($n$=10). An additional 12 undeafened animals served as negative histological controls ($n$=3 each). To determine the timing of S-phase entry in the OC following hair cell injury, 40 animals given BrdU daily from day 2 until days 3, 4, 6, or 8 ($n$=10 each) were killed 12 h after the last BrdU injection (i.e., on days 4, 5, 7, or 9, respectively). Finally, to determine whether BrdU-labeled cells could survive for 1 month, 10 deafened animals were given BrdU for 10 days from day 2 through day 11 and killed on day 31.

The experimental protocol was approved by the University Committee for the Use and Care of Animals at the University of Tokyo and conformed to NIH Guidelines for the Care and Use of Laboratory Animals.

### Deafening with KM and EA and BrdU injection

On day 1, experimental animals were given a single dose of KM (Meiji, Japan; 400 mg/kg, s.c.) and, 2 h later, under general anesthesia induced by intramuscular xylazine hydrochloride at 10 mg/kg (Bayer, Germany) and ketamine hydrochloride at 40 mg/kg (Sankyo, Japan)], they were prepared for cannulation of the jugular vein and injected with EA (50 mg/kg, i.v.), as previously reported (West et al. 1973). BrdU (Sigma, USA) dissolved in sterilized saline (10 mg/ml) was injected (100 mg/kg per injection, i.p.) twice each day at 12-h intervals from day 2 through day 11. The first injection of BrdU was given on day 2, 12 h following the administration of EA.

### ABR measurement

Pure-tone (4, 8, and 20 kHz) ABRs were measured for both ears, 3 days after arrival (before deafening with KM and EA) in all animals and 3 days after deafening (on day 4) in all deafened animals. The method of ABR measurement was as described previously (Yamasoba et al. 1999). In brief, animals were anesthetized with a mixture of xylazine hydrochloride (10 mg/kg, i.m.) and ketamine hydrochloride (40 mg/kg, i.m.), and needle electrodes were placed subcutaneously at the vertex (active electrode), beneath the pinna of the measured ear (reference electrode), and beneath the opposite ear (ground). The stimulus duration was 15 ms, the presentation rate 11/s, and the rise/fall time

1 ms. Responses of 1024 sweeps were averaged at each intensity level (5 dB steps) to assess threshold. Threshold was defined as the lowest intensity level at which a clear reproducible waveform was visible in the trace. When an ABR waveform could not be evoked, threshold was assumed to be 5 dB greater than the maximum intensity produced by the system (105 dB SPL). Threshold shifts were calculated by subtracting baseline thresholds from those on day 4.

### Immunocytochemistry

Animals were killed under deep anesthesia with xylazine and ketamine (as above), and the cochleae from both ears of each animal were perfused intrascalarly with 4% paraformaldehyde in 0.1 M phosphate-buffered saline (PBS) at pH 7.4 and immersed in the same fixative overnight at 4°C. The cochleae were then rinsed in 0.1 M PBS, and the surface of the OC was prepared by removing the otic capsule and tectorial membrane. The dissected specimens were incubated in methanol at −20°C for 20 min, immersed in 2 N HCl for 30 min, and preincubated in 4% normal goat serum in TRIS-buffered saline containing Tween 20 (TBS/T). For labeling with antibodies against p27, cytokeratins, or vimentin, the dissected specimens first were immersed in antigen retrieval solution (DAKO, USA) and microwaved at 95°C for 20 min. The specimens were then incubated overnight at room temperature in a solution containing primary antibodies. After several rinses, these specimens were incubated overnight at room temperature in a solution containing secondary antibodies. After several rinses, each turn of the cochlea was dissected out and mounted on glass slides with Prolong Antifade Kit (Molecular Probes, The Netherlands) and observed under a confocal laser scanning microscope (Axioskop MOT PLUS, Zeiss, Germany). The primary antibodies used were monoclonal rat anti-BrdU (1:500; Bitotech House, UK), monoclonal mouse anti-p27 (sc-1641, 1:200; Santa Cruz Biotechnology, USA), monoclonal mouse anti-pan-cytokeratin (clone PCK-26, 1:200; Sigma, USA), and monoclonal mouse anti-vimentin (clone V9, 1:50; Sigma), and secondary antibodies were fluorescein-isothiocyanate-conjugated affinity-purified goat anti-rat IgG (1:200; Molecular Probes) and rhodamin-conjugated affinity-purified goat anti-mouse IgG (1:200; Molecular Probes). For immunohistochemically negative controls, primary antibodies were omitted from the staining procedure.

Staining with antibodies to cytokeratin and vimentin was chosen because of the presence of both of these in the supporting cells, including the inner pillar cells and Deiters cells (DCs), but not in the hair cells in the mature guinea pig cochlea. Cytokeratins are present in the apical domain at the reticular lamina and in the basal domain near the basilar membrane in the supporting cells in normal cochlea and fill the expanded apical portions of the DCs in ototoxically damaged cochlea (Oesterle et al. 1990; Raphael and Altschuler 1991). Vimentin immunostaining is present in the cytoplasm of the third-row DCs, in the perinuclear region of the first-row and second-row DCs, and in the apical portion of the inner pillar cells. In general, vimentin is absent in the phalangeal scar when hair cells are destroyed by intense noise or ototoxic agents (Oesterle et al. 1990; Raphael and Altschuler 1991). Staining with antibodies to p27 was chosen because of the expression of this protein in the nuclei of the supporting cells of the OC (Chen and Segil 1999; Chen et al. 2002; Endo et al. 2002).

### Observation of sections cut perpendicular to the basilar membrane

The dissected cochlear sensory epithelia were incubated with 3% $H_2O_2$ in methanol at −20°C for 30 min, immersed in 2 N HCl for 30 min, rinsed in PBS, and then incubated overnight at room temperature in a solution containing mouse monoclonal antibody to BrdU (Clone Bu20a; 1:500; DAKO, Denmark). After several rinses, these specimens were incubated overnight with a peroxidase-conjugated secondary antibody (Histofine, simple stain PO Max [Multi], Nichirei, Japan). They were then rinsed several times and allowed to react with DAB (Histofine, simple stain DAB; Nichirei, Japan). Each turn of the cochlea was mounted on a glass slide with aqueous/dry mounting medium (Crystal/mount, Biomeda, USA) and observed by Nomarski optics to detect BrdU-labeled nuclei in the OC. Turns including BrdU-labeled nuclei in the OC were then postfixed in 1% osmium tetroxide for 2 h, dehydrated in a graded alcohol series, and embedded in Epoxy resin. Consecutive sections of the embedded specimens, which were approximately 1 μm thick and perpendicular to the basilar membrane, were obtained, counterstained with toluidine blue, mounted on glass slides, and observed under Nomarski optics. Ultrathin sections of the specimens containing BrdU-labeled nuclei were then obtained, stained with uranyl acetate and lead citrate, and observed by TEM (H-800, Hitachi, Japan). The normal OC in three undeafened animals was processed similarly and served as a control.

## Results

### ABR findings in deafened animals

In all of the deafened animals, ABR measurement performed on day 4 showed significant increases of ABR thresholds, compared with the predeafening baseline measure. The mean threshold shifts (±SD) were 53±14, 62±18, and 68±14 dB at 4, 8, and 20 kHz, respectively. None of the animals showed ABR threshold shifts smaller than 30 dB at any frequencies examined.

Detection of BrdU-labeled cells in the OC in deafened animals given BrdU for 10 days

By 10 days following administration of KM and EA, the OHCs were destroyed nearly totally in the basal and second turns, moderately to severely in the third turn, and mildly in the apical turn, whereas almost all the IHCs and supporting cells throughout the OC remained intact. When lost, the OHCs were replaced by a phalangeal scar (Fig. 1a,j). This finding and the extent of ABR threshold shifts were similar

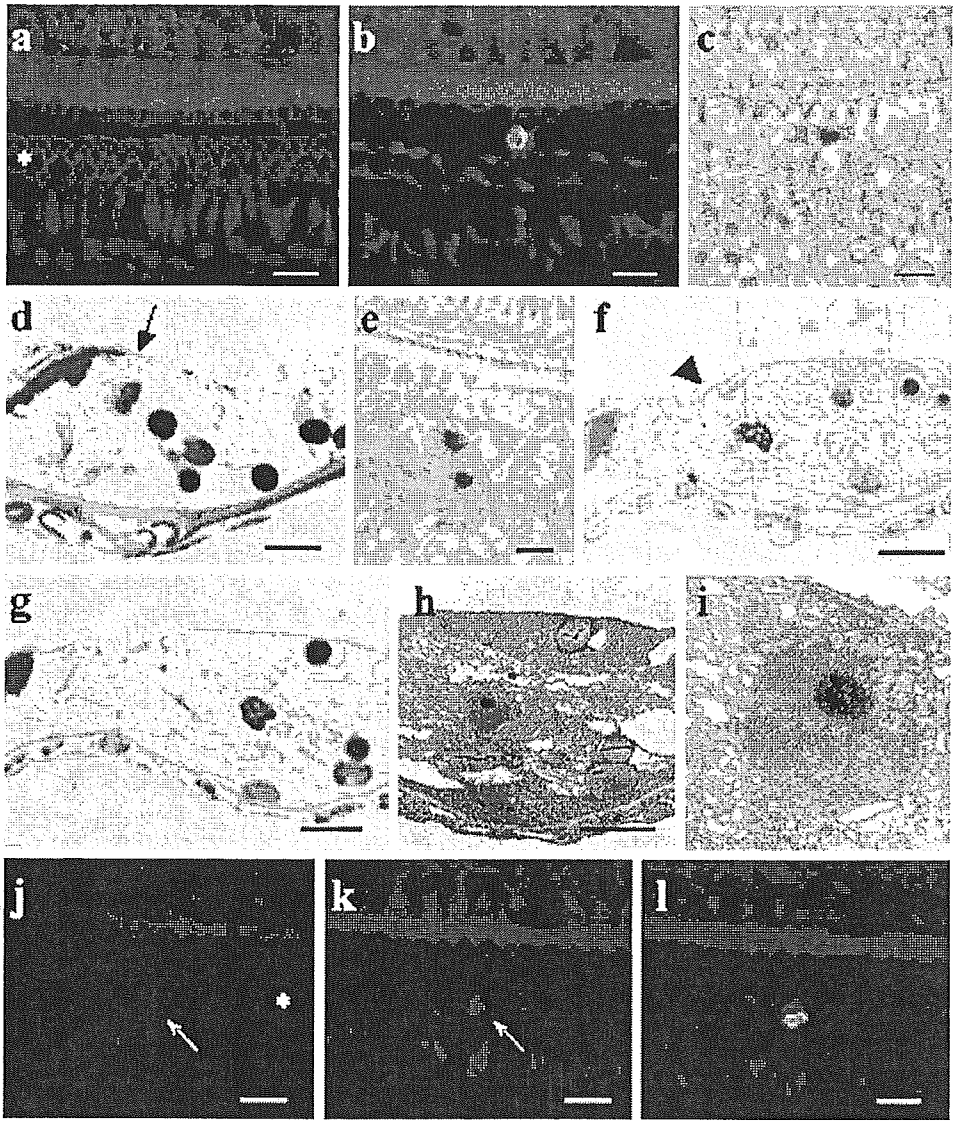


**Fig. 1** **a–i** Organ of Corti (OC) of deafened animals given BrdU for 10 days. **a** In the apical surface of a whole-mount surface preparation of the OC, one inner hair cell is missing and all the outer hair cells (OHCs) are replaced by phalangeal scars (*asterisk*). **b** Below the scar shown in **a**, a single BrdU-labeled nucleus is observed in the first-row Deiters cell (DC). **c** An isolated single BrdU-labeled nucleus in the region of the first-row DCs in a whole-mount surface preparation of the OC. **d** Lateral view of the specimen shown in **c** demonstrates a BrdU-labeled cell located at a level normally occupied by the OHCs, with its superior portion extending to the reticular lamina (*arrow*) but containing no cuticular plate. **e** BrdU-labeled nuclei located in the region of second-row DCs in a whole-mount surface preparation of the OC. **f, g** Lateral views of specimen shown in **e** demonstrating labeled nucleus (**g**) located at a level normally occupied by nuclei of DCs and a second nucleus (**f**) nearer the reticular lamina. The superior portion of the latter reaches to the reticular lamina (*arrowhead*). **h,i** Low (**h**) and high (**i**) magnification transmission electron micrographs of the section shown in **g** demonstrating that the BrdU-labeled nucleus shows no sign of apoptosis. **j–l** The OC of deafened animals given BrdU for 5 days. **j** In the apical surface of a whole-mount surface preparation of the OC, all the OHCs are replaced by phalangeal scars (*asterisk*). The phalangeal scar of the cell containing BrdU-positive nuclei shown in **l** is indicated (*arrow*). **k** Approximately 6 μm below the section shown in **j**. DCs are present and exhibit expansion of their phalangeal processes (*arrow* phalangeal process of the cell containing BrdU-positive nuclei shown in **l**). **k** Approximately 12 μm below the section shown in **j**. BrdU-positive segregating daughter nuclei are present in the second-row DC. *Bars* 10 μm

to those reported by Izumikawa et al. (2005). In these animals, BrdU-labeled cells were frequently seen in tissues outside of the OC, such as fibroblasts and red blood cells in capillaries beneath the basilar membrane (data not shown). This staining, outside the OC, was also observed in undeafened controls, although the number of BrdU-labeled cells outside the OC was significantly smaller in controls compared with animals treated with KM and EA, as previously observed (Yamasoba et al. 2003). The BrdU staining outside the OC served as an internal positive control, ensuring that the BrdU, its antibody, and the secondary markers had reached the cochlea. Surprisingly, at least one BrdU-labeled nucleus was observed in the OC in 11 (55%) of 20 ears (Figs. 1b, 2); the number of BrdU-labeled nuclei ranged from 0 to 10 (3.6±3.1) per ear. BrdU-labeled nuclei were observed beneath the scar, most commonly in the regions of the first-row and second-row DCs and occasionally in the regions of the third-row DCs. Only a few labeled nuclei were observed in the regions of the outer pillar cells and Hensen cells. Most of BrdU-labeled nuclei were located within cells that demonstrated an upper portion projecting to the reticular lamina. Approximately one-third of BrdU-labeled nuclei were closely located, as pairs, whereas the remaining two-thirds were isolated, as single nuclei. Clusters of more than two labeled cells were not observed. BrdU-labeled nuclei were commonly observed in the lower three turns of the cochlea (Fig. 2), probably because the OHCs were damaged more severely in these turns. In control animals, no BrdU-labeled nuclei were observed within the normal OC. When the primary antibody was omitted from the immunohistochemical staining procedure, no labeled nuclei were present in any of the tissues examined (data not shown).

## Lateral view of the BrdU-labeled cells in the OC

Lateral views of the OC demonstrated that BrdU-labeled nuclei were located commonly in the mid regions, at a level normally occupied by the nuclei of the DCs (Fig. 1e–i), and in some cases more apically (i.e., toward the reticular lamina), approximating the level normally occupied by the nuclei of the OHCs (Fig. 1c,d). The apical portions of cells containing BrdU-labeled nuclei were commonly extended to the reticular lamina but had no cuticular plate. Ultrathin sections of these specimens showed that all organelles were somewhat compromised by technical artifacts reflecting the use of 4% paraformaldehyde alone and repeated mounting. These degenerative changes were observed in all cells of the OC and in both control (data not shown) and experimental material, indicating that they were not drug-induced damage. We found no clear indication of apoptosis, such as nuclear condensation (Fig. 1h,i), in this material. However, given the BrdU-induced damage (artifacts) to nuclear structures, it was difficult to conclude that apoptotic processes were not involved.

## Double-staining with BrdU and p27, cytokeratin, or vimentin

Labeling with antibodies against p27 showed that the protein was expressed only in supporting cells and not in hair cells in the normal controls (data not shown), as previously reported (Chen and Segil 1999; Chen et al. 2002; Endo et al. 2002). In the deafened animals, BrdU-labeled nuclei in the OC were also labeled with p27 (Fig. 3a–c), and cytokeratins filled the expanded apical portions of DCs (Fig. 3d–f). Vimentin strongly labeled the cytoplasm of the third-row DCs and inner pillar cells and more faintly the perinuclear regions in the first-row and second-row DCs (Fig. 3g–i). The pattern of staining of these intermediate filaments was similar to that previously observed in the damaged cochlea (Oesterle et al. 1990; Raphael and Altschuler 1991). BrdU-labeled nuclei were located beneath the cytokeratin-positive apical portion of the DCs and in vimentin-positive cytoplasm in the DCs (Figs. 2, 3d–i). Vimentin was more strongly stained in the perinuclear regions of the first-row and second-row DCs labeled by BrdU compared with those unlabeled by BrdU. When two paired BrdU-labeled nuclei were found, one nucleus was commonly located in the inferior portion of

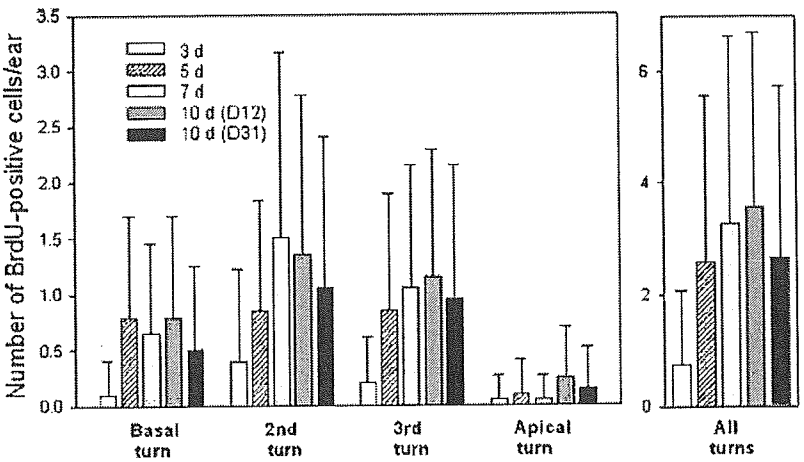


**Fig. 2** Number (average±SD) of BrdU-labeled nuclei in the basal, second, third, and apical turns and the sum of these in animals deafened by administration of kanamycin sulfate and ethacrynic acid on day 1 and given BrdU from day 2 for 3 ($n$=10), 5 ($n$=10), 7 ($n$=10) or 10 ($n$=20) days. Animals given BrdU for 7 days or less were killed 12 h after the last BrdU injection, and those given BrdU for 10 days were killed on day 12, 12 h after the last BrdU injection ($n$=10) or on day 31 ($n$=10)

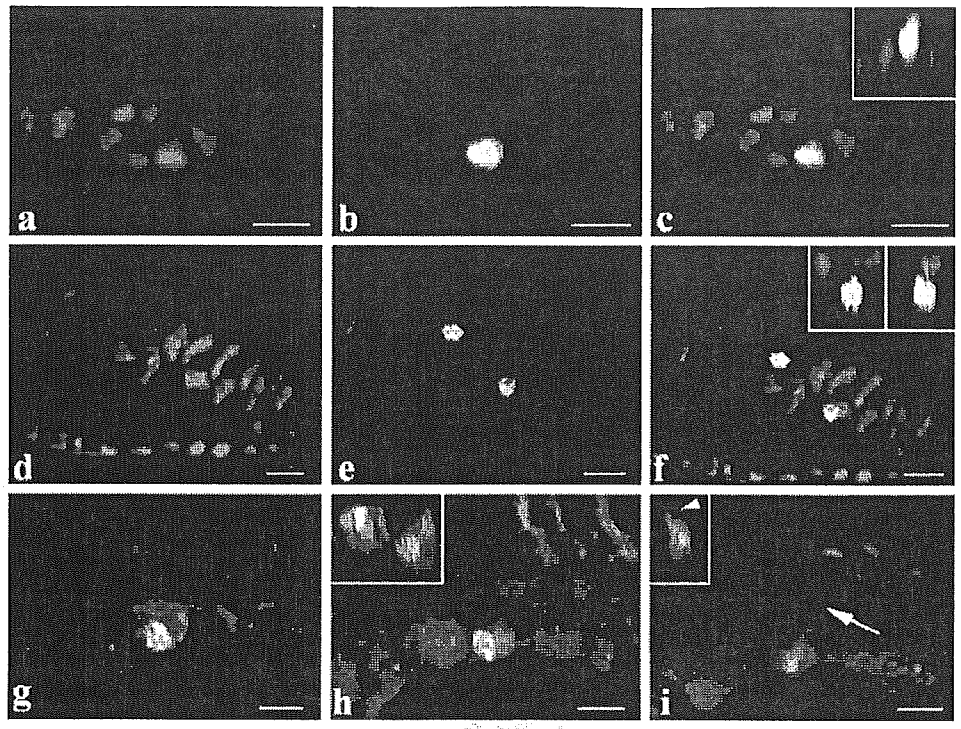


**Fig. 3** Double-staining with antibodies against BrdU and p27 (**a–c**), cytokeratins (**d–f**), or vimentin (**g–i**) in whole-mount surface preparations of the OC of deafened animals given BrdU for 10 days. **a** Nuclei of the first-row and second-row DCs are labeled with p27. **b** One BrdU-labeled nucleus is present in a second-row DC. **c** The merged view and ortho-image of these slices (*inset*) show that the BrdU-labeled nucleus is also labeled with p27. **d** The expanded apical portions of the DCs are labeled with cytokeratins. **e** Two BrdU-labeled nuclei are present in the regions of first-row and second-row DCs. **f** The merged view and ortho-images of these slices (*insets*) show that BrdU-labeled nuclei are located beneath the apical portions of the DCs. **g** One BrdU-labeled nucleus in the first-row DC is present slightly beneath the reticular lamina. Vimentin is stained in the regions around the BrdU-labeled nuclei. **h** Another BrdU-labeled nucleus is present in vimentin-positive cytoplasm of an adjacent DC (*inset* ortho-image of these slices). **i** Approximately 6 μm below the section shown in **h**, vimentin is more faintly stained in the cytoplasm of DCs unlabeled by BrdU. The phalangeal process (*arrow*; *arrowhead* in *inset*) obliquely projects from the BrdU-labeled DC. *Bars* 10 μm

vimentin-positive cytoplasm of the DC and the second in the more apical portion of the neighboring DCs (Fig. 3g–i).

### Timing of appearance of BrdU-labeled cells following injection with KM and EA

Because a total of 20 injections of BrdU over a 10-day period resulted in only the limited uptake of BrdU in the OC after ototoxic insults, we considered it impossible to identify the timing of S phase after hair cell injury by a single injection of BrdU. We therefore adopted a strategy of applying cumulative BrdU, by injections over different courses of treatment. BrdU-labeled nuclei were absent in the OC in all animals given BrdU for only 2 days. A small number of the BrdU-labeled nuclei were first detected in the OC of animals given BrdU for 3 days. The number of BrdU-labeled nuclei significantly increased when BrdU was given for 5 days and did not significantly change thereafter (Fig. 2). We also found a DC that contained segregating BrdU-positive daughter nuclei in an animal given BrdU for 5 days (Fig. 1j–l).

### Survival of BrdU-labeled cells

When animals were given BrdU for 10 days and killed on day 31, almost all the OHCs were missing and replaced by a phalangeal scar in the second and third turns, whereas damage to the OHCs in the apical turn was mild to moderate. In the basal turn, no OHCs were observed in any of the animals, and the OC was commonly collapsed. At least one BrdU-labeled nucleus was observed in the OC in 10 (50%) out of 20 ears. The number of BrdU-labeled nuclei ranged from 0 to 8 (2.7±3.1) per ear, which was not significantly different from that (3.6±3.1 per ear) in animals given BrdU for 10 days and killed on day 12 (Fig. 2). These findings indicated that BrdU-labeled cells could survive at least for 1 month.

## Discussion

Following administration of KM and EA, we observed limited numbers of BrdU-labeled nuclei in the regions of the DCs in the mature OC of the young guinea pig. BrdU-

labeled nuclei were commonly observed in the basal, second, and third turns, but very rarely in the apical turn, probably because the OHCs were damaged severely in the lower three turns but mildly to moderately in the apical turn. BrdU-labeled nuclei were located at the regions in which the nuclei of the DCs were normally present, or more apically, at a level normally occupied by the nuclei of the OHCs. The apical portions of BrdU-labeled cells typically demonstrated a DC-like phalangeal process extending to the reticular lamina. BrdU-labeled nuclei were also labeled with p27 and located within the vimentin-positive cytoplasm of the DCs and beneath the cytokeratin-positive expanded apical portion of these cells. These findings indicate that the original sets of cells containing BrdU-labeled nuclei are the DCs.

Nonspecific uptake of BrdU might however have occurred passively in cells with severely damaged DNA, when the cells were in the process of dying. However, several pieces of evidence exclude this possibility. First, administration of KM and EA induced severe damage to the OHCs acutely within a few days, whereas the damage to the IHCs and supporting cells was minimal, as previously observed (West et al. 1973; Yamasoba et al. 2003). Second, animals were killed at least 12 h following the last BrdU injection, which is considered long enough to allow apoptotic cells labeled with BrdU to be removed. Histologically visible stages of the apoptotic process are known to be short, lasting from a few minutes to a maximum of 3 h (Bursch et al. 1990). Although the rate of removal of dead cells may vary in different tissues, previous evaluations in the developing nervous system suggest that this occurs rapidly, within a few hours (Voyvodic et al. 1995; Thomaidou et al. 1997). Third, the number of BrdU-labeled nuclei did not significantly differ between animals given BrdU for 10 days and killed on day 12 and day 31. These findings argue against the BrdU-labeled nuclei observed in the OC having been nonspecifically labeled while being involved in cell death.

The current study revealed that the number of BrdU-labeled nuclei in the OC was small after ototoxic insults. However, we injected BrdU every 12 h. Since BrdU is cleared within approximately 2 h (Matei et al. 2005), BrdU should be injected every 2 h, as shown by Chen et al. (2002), to label all or most proliferating cells. However, given the toxic side-effects of BrdU, such repeated injections would only be tolerable if animals were allowed to survive for a short period. Given the longer survival time required in this study, ethical approval could not be obtained for the repeated higher daily concentrations of BrdU required to capture all cells. Thus, our current assessment is probably conservative, and many more proliferating cells (approximately 6×) might have been observed with more frequent BrdU injections. Even if we only labeled approximately 1/6 of the possible proliferating cells, the proliferation activity of the supporting cells in the OC after hair cell loss still appears limited. In the utricular macula of guinea pig, continuous infusion of cell proliferation marker in vivo for one to several weeks has also revealed that a single injection of gentamicin into the middle ear spaces induces limited cell proliferation (e.g., fewer than 12 labeled cells/utricle; Rubel et al. 1995; Li and Forge 1997). Following gentamicin treatment, a total of 23 $^{3}$H-thymidine-labeled supporting cells were observed in four of seven animals (Rubel et al. 1995) and a total of 18 BrdU-labeled nuclei were observed in three of four animals (Li and Forge 1997). These findings suggest that, following ototoxic insults in guinea pigs, cell proliferation may be limited both in the cochleae and in vestibular endorgans.

Cumulative BrdU injection for diverse lengths has revealed that the uptake of BrdU occurs most robustly in the guinea pig OC 3–5 days following hair cell injury. This time window of BrdU uptake is similar to that in chick basilar papilla following insults by systemic aminoglycoside injection; pulse/fix BrdU labeling studies have shown a dramatic increase in BrdU-labeled cells at 3 days following a single systemic injection of gentamicin, and the number of labeled cells decreases rapidly by 5 days following the injection (Bhave et al. 1995; Stone et al. 1999).

When BrdU-labeled nuclei were detected in deafened animals given BrdU for 10 days, closely paired labeled nuclei were observed in approximately one-third of cases. We also found a DC containing BrdU-labeled daughter nuclei, suggesting segregation during mitosis, in an animal given BrdU for 5 days. The presence of the pairs of BrdU-labeled nuclei and a segregating daughter nuclei in the DC suggested that these labeled cells were in S phase at the time of BrdU injection and were able to pass through the $G_2$ and M phases before analysis. Clusters of more than two labeled cells were not observed, suggesting that the DCs that had taken up BrdU did not go on to divide more than once.

In the deafened animals, BrdU-labeled nuclei in the OC were co-labeled with p27, suggesting that the DCs that had taken up BrdU had exited the cell cycle prior to analysis. It is of importance to understand how these cells can enter the cell cycle, while expressing this negative cell cycle regulator. Fibroblasts still express p27 when they are actively proliferating, although its expression is reduced (Malek et al. 2001). This finding indicates that the presence of p27 in BrdU-positive cells does not mean that they are incapable of cell cycle re-entry. Mice that are heterozygous for the p27 mutation ($p27^{+/-}$), and that contain about 50% of the p27 found in wild-type littermates (Kil et al. 2000) occasionally exhibit supernumerary IHCs (Chen and Segil 1999) but show an increase of BrdU-positive cells in the OC after significant hair cell loss induced by systemic amikacin injection (Kil et al. 2000). These findings suggest that cochlear supporting cells are able to proliferate when p27 is downregulated below a certain level, and that hair cell loss can trigger this proliferation. Positivity for p27 significantly decreases in the DC after topical application of cisplatin to mice; cisplatin kills most OHCs but not DCs (Endo et al. 2002). In view of these observations, we speculate that significant hair cell loss induced by KM and EA may have induced significant downregulation of p27 below a critical level in some DCs, which then enter cell cycle.

Why only a proportion of BrdU-labeled cells has been demonstrated as paired doublets in the damaged OC of guinea pigs, and similarly in the utricular macula of gentamicin-treated guinea pigs in vivo, remains unknown. Rubel et al. (1995) have found only three labeled doublets out of 23 $^{3}$H-thymidine labeled supporting cells. Perhaps only a proportion of BrdU-labeled supporting cells might enter $G_2$ and then M phase after S phase. Another possibility is that some daughter cells may die shortly after division in the inner ear. In the developing or proliferating central or peripheral nervous system, cell death commonly occurs shortly after the replication of DNA or on exiting the cell cycle (Barres et al. 1992; Yaginuma et al. 1996; Thomaidou et al. 1997). Moreover, mice lacking the retinoblastoma gene (*Rb1*), a negative regulator of the cell cycle, show continued proliferation of hair cells and supporting cells, some of which differentiate whereas others degenerate (Mantela et al. 2005).

When we found two paired BrdU-labeled nuclei were found, one was commonly located at a level normally occupied by the nuclei of the DCs and its sister nucleus occurred more apically at a level normally occupied by the nuclei of the OHCs. When paired labeled nuclei were observed in the vimentin-positive cell bodies, typically one was located in the inferior portion of the vimentin-positive cytoplasm of the DCs and second in the superior portion of vimentin-positive cytoplasm of the adjacent sister DCs. These findings suggested that BrdU-labeled nuclei located apically at a level normally occupied by the nuclei of the OHCs had migrated from their original position. Vimentin was faintly stained in the DCs not expressing BrdU but was more strongly stained in the DCs labeled by BrdU, indicative that vimentin synthesis was upregulated in the BrdU-labeled DCs. This is consistent with findings that vimentin is associated with the mitotic apparatus and related to the induction of cellular DNA synthesis or mitosis, and that increases in vimentin synthesis are associated with rapidly growing cells, because of its involvement in the extensive remodeling of cytoskeletal components required for mitosis, migration, and process outgrowth (Baserga 1985; Ferrari et al. 1986). Following hair cell injury, vertical migration of the nuclei labeled with cell proliferation marker has been observed in chick basilar papilla (Stone and Cotanche 1994; Stone and Rubel 2000), in which proliferated sister cell pairs go on to differentiate as a supporting cell and a hair cell, as two supporting cells, or as two hair cells in the chick basilar papilla (Stone and Rubel 2000). We are currently examining whether the DCs that migrate apically after cell division can differentiate to hair cells.

Conceptually, there are several possible ways to attempt the generation of (or introduction of) new hair cells to restore the function of the OC. These include (1) the generation of new cells by mitosis of supporting cells (with some of the progeny differentiating into new hair cells), (2) the conversion of the phenotype of supporting cells to hair cells (with or without mitosis), or (3) the implantation of stem cells or other progenitors that will differentiate to new hair cells. Several lines of research have been conducted for possible interventions to accomplish these goals. For example, in vivo inoculation of adenovirus encoding the *Atoh1* gene into the endolymph of the mature guinea pig cochlea results in the production of new hair cells (Kawamoto et al. 2003; Izumikawa et al. 2005), indicative that nonsensory cells in the mature mammalian cochlea can generate new hair cells after overexpression of genes that are necessary and sufficient for hair cell differentiation. However, in the avian inner ear, the generation of new cells occurs spontaneously, without any therapeutic intervention, via the mitosis of supporting cells: hair cell injury induces supporting cells to become precursors, to re-enter the cell cycle, and to provide daughter cells that become new hair cells (Corwin and Cotanche 1988; Ryals and Rubel 1988; Stone and Cotanche 1994; Bhave et al. 1995; Stone et al. 1999; Stone and Rubel 2000). Our current study demonstrates that at least the first phase of avian hair cell regeneration is indeed possible in the mammal cochlea. A more limited regenerative response has also been observed in the vestibular organs of mammals, in which the reoccurrence of hair cells also reflects supporting cell proliferation (Forge et al. 1993; Rubel et al. 1995; Kuntz and Oesterle 1998). In developing mice lacking p27, a critical factor in cell cycle arrest, cells of the OC continue to proliferate for more than 2 weeks after normal cessation, and supporting cells can generate new hair cells after trauma-induced hair cell loss (Chen and Segil 1999; Raphael 2002), indicating that supporting cells in the mammalian cochlea can differentiate spontaneously into hair cells when they re-enter the cell cycle. The current study has also demonstrated that mature DCs have an albeit limited competence to re-enter the cell cycle and proliferate. If we can enhance cell proliferation of these supporting cells following hair cell injury, we may generate a large enough precursor cell pool to regenerate the mature mammalian cochleae. Presumably, the induction of several mitogenic growth factors that enhance cell proliferation in the mammalian vestibular sensory epithelia or the down-regulation of molecules, such as *p27*, that inhibit cell re-cycling in supporting cells (Kil et al. 2000) may achieve this goal. Interestingly, we have recently observed that inoculation of adenovirus encoding shRNA, which targets p27kip1 mRNA into the deafened guinea pig cochlea, induces supporting cell proliferation and new stereociliary bundles in vivo (unpublished).

**Acknowledgements** We are grateful to Drs. Josef M. Miller, Joseph E. Hawkins, Yasuya Nomura, and Masato Nakafuku for helpful comments and discussion and to Mr. Yoshiro Mori, Mr. Ko-ichi Miyazawa, Ms. Atsuko Tsuyuzaki, Ms. Yukari Kurasawa, and Dr. Shinichi Ishimoto for technical support.

## References

Barres BA, Hart IK, Coles HSR, Burne JF, Voyvodic JT, Richardson WD, Raff MC (1992) Cell death and control of cell survival in the oligodendrocyte lineage. Cell 70:31–46

Baserga R (1985) The biology of cell reproduction. Harvard University Press, Cambridge

Bermingham-McDonogh O, Rubel EW (2003) Hair cell regeneration: winging our way towards a sound future. Curr Opin Neurobiol 13:119–126

Bhave SA, Stone JS, Rubel EW, Coltrera MD (1995) Cell cycle progression in gentamicin-damaged avian cochleas. J Neurosci 15:4618–4628

Bursch W, Kleine L, Tenniswood M (1990) The biochemistry of cell death by apoptosis. Biochem Cell Biol 68:1071–1074

Chardin S, Romand R (1995) Regeneration and mammalian auditory hair cells. Science 267:707–711

Chen P, Segil N (1999) p27(Kip1) links cell proliferation to morphogenes in the developing organ of Corti. Development 126:1581–1590

Chen P, Johnson JE, Zoghbi HY, Segil N (2002) The role of Math1 in inner ear development: uncoupling the establishment of the sensory primordium from hair cell fate determination. Development 129:2495–2505

Corwin T, Cotanche DA (1988) Regeneration of sensory hair cells after acoustic trauma. Science 240:1772–1774

Endo T, Nakagawa T, Lee JE, Dong Y, Kim TS, Iguchi F, Taniguchi Z, Naito Y, Ito J (2002) Alteration in expression of p27 in auditory epithelia and neurons of mice during degeneration. Neurosci Lett 334:173–176

Ferrari S, Battini R, Kaczmarek L, Rittling S, Calabretta B, Riel JK de, Philiponis V, Wei JF, Baserga R (1986) Coding sequence and growth regulation of the human vimentin gene. Mol Cell Biol 6:3614–3620

Forge A, Li L, Corwin JT, Nevill G (1993) Ultrastructural evidence for hair cell regeneration in the mammalian inner ear. Science 259:1616–1619

Izumikawa M, Minoda R, Kawamoto K, Abrashkin KA, Swiderski DL, Dolan DF, Brough DE, Raphael Y (2005) Auditory hair cell replacement and hearing improvement by Atoh1 gene therapy in deaf mammals. Nat Med 11:271–276

Kawamoto K, Ishimoto S, Minoda R, Brough DE, Raphael Y (2003) Math1 gene transfer generates new cochlear hair cells in mature guinea pigs in vivo. J Neurosci 23:4395–4400

Kil J, Gu R, Zhao YD, Hasson T, Lowenheim H, Fero M (2000) Inhibition of p27Kip1 induces hair cell regeneration in the organ of Corti. Assoc Res Otolaryngol Abstr 23:5510

Kuntz AL, Oesterle EC (1998) Transforming growth factor alpha with insulin stimulates cell proliferation in vivo in adult rat vestibular sensory epithelium. J Comp Neurol 399:413–423

Lang H, Fekete DM (2001) Lineage analysis in the chicken inner ear shows differences in clonal dispersion for epithelial, neuronal, and mesenchymal cells. Dev Biol 234:120–137

Lefebvre PP, Malgrange B, Staecker H, Moonen G, Van de Water TR (1993) Retinoic acid stimulates regeneration of mammalian auditory hair cells. Science 260:692–695

Li L, Forge A (1997) Morphological evidence for supporting cell to hair cell conversion in the mammalian utricular macula. Int J Dev Neurosci 15:433–446

Malek NP, Sundberg H, McGrew S, Nakayama K, Kyriakides TR, Roberts JM (2001) A mouse knock-in model exposes sequential proteolytic pathways that regulate p27Kip1 in G1 and S phase. Nature 413:323–327

Mantela J, Jiang Z, Ylikoski J, Fritzsch B, Zacksenhaus E, Pirvola U (2005) The retinoblastoma gene pathway regulates the postmitotic state of hair cells of the mouse inner ear. Development 132:2377–2388

Matei V, Pauley S, Kaing S, Rowitch D, Beisel KW, Morris K, Feng F, Jones K, Lee J, Fritzsch B (2005) Smaller inner ear sensory epithelia in Neurog1 null mice are related to earlier hair cell cycle exit. Dev Dyn 234:633–650

Oesterle EC, Sarthy PV, Rubel EW (1990) Intermediate filaments in the inner ear of normal and experimentally damaged guinea pigs. Hear Res 47:1–16

Raphael Y (2002) Cochlear pathology, sensory cell death and regeneration. Br Med Bull 63:25–38

Raphael Y, Altschuler RA (1991) Scar formation after drug-induced cochlear insult. Hear Res 51:173–183

Roberson DW, Rubel EW (1994) Cell division in the gerbil cochlea after acoustic trauma. Am J Otol 15:28–34

Rubel EW, Dew LA, Roberson W (1995) Mammalian vestibular hair cell regeneration. Science 267:701–707

Ruben RJ (1967) Development of the inner ear of the mouse: a radioautographic study of terminal mitoses. Acta Otolaryngol Suppl 220:1–44

Ryals BM, Rubel EW (1988) Hair cell regeneration after acoustic trauma in adult *Coturnix* quail. Science 240:1774–1776

Slepecky NB (1996) Structure of the mammalian cochlea. In: Dallos P, Popper AN, Fay RR (eds) The cochlea. Springer, Berlin Heiderberg New York, pp 46–129

Stone JS, Cotanche DA (1994) Identification of the timing of S phase and the patterns of cell proliferation during hair cell regeneration in the chick cochlea. J Comp Neurol 341:50–67

Stone JS, Rubel EW (2000) Temporal, spatial, and morphologic features of hair cell regeneration in the avian basilar papilla. J Comp Neurol 417:1–16

Stone JS, Choi YS, Woolley SM, Yamashita H, Rubel EW (1999) Progenitor cell cycling during hair cell regeneration in the vestibular and auditory epithelia of the chick. J Neurocytol 28:863–876

Thomaidou D, Mione MC, Cavanagh JFR, Parnavelas JG (1997) Apoptosis and its relation to the cell cycle in the developing cerebral cortex. J Neurosci 17:1075–1085

Voyvodic JT, Burne JF, Raff MC (1995) Identification of normal cell death in the rat retina: applications for normal composition in cell lineage analysis. Eur J Neurosci 7:2469–2478

West RA, Brummett RE, Himes DL (1973) Interaction of kanamycin and ethacrynic acid. Severe cochlear damage in guinea pigs. Arch Otolaryngol 98:32–37

Yaginuma H, Tomita M, Takashita N, McKay SE, Cardwell C, Yin Q-W, Oppenheim RW (1996) A novel type of programmed neuronal death in the cervical spinal cord of the chick embryo. J Neurosci 16:3685–3703

Yamasoba T, Schacht J, Shoji F, Miller JM (1999) Attenuation of cochlear damage from noise trauma by an iron chelator, a free radical scavenger and glial cell line-derived neurotrophic factor in vivo. Brain Res 815:317–325

Yamasoba T, Kondo K, Miyajima C, Suzuki M (2003) Changes in cell proliferation in rat and guinea pig cochlea after aminoglycoside-induced damage. Neurosci Lett 347:171–174

# MIDAS/GPP34, a nuclear gene product, regulates total mitochondrial mass in response to mitochondrial dysfunction

**Naomi Nakashima-Kamimura[1], Sadamitsu Asoh[1], Yoshitomo Ishibashi[1], Yuri Mukai[1,*], Yujiro Shidara[1,2], Hideaki Oda[2], Kae Munakata[3], Yu-ichi Goto[3] and Shigeo Ohta[1,‡]**

[1]Department of Biochemistry and Cell Biology, Institute of Development and Aging Sciences, Graduate School of Medicine, Nippon Medical School, 1-396 Kosugi-cho, Kawasaki, Kanagawa, 211-8533, Japan
[2]Department of Pathology, Tokyo Women's Medical University, School of Medicine, Shinjuku-ku, Tokyo, 162-8666, Japan
[3]Department of Mental Retardation and Birth Defect Research, National Institute of Neuroscience, NCNP, Kodaira, Tokyo, 187-8502, Japan
*Present address: Computational Biology Research Center (CBRC), National Institute of Advanced Industrial Science and Technology (AIST), Koutou-ku, Tokyo, 135-0064, Japan
‡Author for correspondence (e-mail:ohta@nms.ac.jp)

*Accepted 15 August 2005*
*Journal of Cell Science 118, 000-000 Published by The Company of Biologists 2005*
*doi:10.1242/jcs.02645*

## Summary

**To investigate the regulatory system in mitochondrial biogenesis involving crosstalk between the mitochondria and nucleus, we found a factor named MIDAS (mitochondrial DNA absence sensitive factor) whose expression was enhanced by the absence of mitochondrial DNA (mtDNA). In patients with mitochondrial diseases, MIDAS expression was increased only in dysfunctional muscle fibers. A majority of MIDAS localized to mitochondria with a small fraction in the Golgi apparatus in HeLa cells. To investigate the function of MIDAS, we stably transfected HeLa cells with an expression vector carrying *MIDAS* cDNA or siRNA. Cells expressing the MIDAS protein and the siRNA constitutively showed an increase and decrease in the total mass of mitochondria, respectively, accompanying the regulation of a mitochondria-specific phospholipid, cardiolipin. In contrast, amounts of the mitochondrial DNA, RNA and proteins did not depend upon MIDAS. Thus, MIDAS is involved in the regulation of mitochondrial lipids, leading to increases of total mitochondrial mass in response to mitochondrial dysfunction.**

Supplementary material available online at
http://jcs.biologists.org/cgi/content/full/118/22/5357/DC1

Key words: Mitochondria, Mitochondrial mass, Cardiolipin, Mitochondrial DNA, Mitochondrial disease, Golgi apparatus

## Introduction

The mitochondrion is the center of energy metabolism in eukaryotes and has recently been recognized as a multifunctional organelle (Ohta, 2003). It is involved in the regulation of apoptosis as a reservoir of signals, regulators and executioners (Kroemer and Reed, 2000; Green and Kroemer, 2004). In addition, it functions as a source of reactive oxygen species, which are believed to cause many lifestyle-related diseases, neurodegenerative diseases, cancer and aging (Kowaltowski and Vercesi, 1999; Cortopassi and Wong, 1999; Melov, 2000). Thus, mitochondria are essential in many aspects of medicine as well as cell biology.

Depending on cell type, energy demands and physiological conditions, mitochondria vary in number, mass and morphology (Attardi and Schatz, 1988; Yaffe, 1999; Collins et al., 2002; Nisoli et al., 2003). The proliferation of cells usually accompanies an increase in mitochondria. However, an increase in number of mitochondria is not distinctly coordinated with the cell cycle. For example, muscle mitochondria increase in response to exercise, independently of cell division (Brunk, 1981; Moyes et al., 1997). Exposure to a low-temperature environment or cultivation in glucose-deprived medium induces a marked increase in mitochondrial mass (Klaus et al., 1991; Weber et al., 2002). In addition, mitochondria increase in response to external stimuli with a wide range of substances including benzodiazepine, phorbol esters, calcium fluxes (Bereiter-Hahn and Voth, 1994; Vorobjev and Zorov, 1983; Muller-Hocker et al., 1986; Kawahara et al., 1991), thyroid hormones (Goglia et al., 1999) and nitric oxide (NO) (Nisoli et al., 2004). Mitochondrial numbers also increase in response to internal stimuli, such as the mitochondrial dysfunction caused by pathogenic mtDNA mutations (Schon, 2000; Wallace, 1999; Moraes et al., 1992). An increase in mitochondrial mass was observed in mitochondrial transcription factor A (*Tfam*) knockout mice, which have depleted mtDNA (Hansson et al., 2004).

As nuclear genes encode most mitochondrial proteins, including the enzymes and cofactors required for the transcription and replication of mtDNA, mitochondrial biogenesis depends on a distinct crosstalk between two physically separated genetic systems (Garesse and Vallejo, 2001). Recently, the pathway that links external physiological stimuli to the regulation of mitochondrial biogenesis and function has been studied. Several transcription/replication factors directly regulate mitochondrial genes and the

coordination of these factors into a programmed response to the environment was reported (Scarpulla, 2002).

However, the nature of mitochondrial biogenesis in response to internal stimuli is poorly understood. Mitochondrial stress results in enhanced expression of sarcoplasmic reticular ryanodine receptor-1 and some $Ca^{2+}$-responsive transcription factors (Biswas et al., 1999). Several tumor-specific markers are overexpressed in cells subjected to mitochondrial genetic as well as metabolic stress (Amuthan et al., 2001). Moreover, we have reported that expression of the apoptosis-mediator Fas is enhanced by dysfunctional mitochondria (Asoh et al., 1996). However, no one has reported on the mammalian factors, in response to a signal from mitochondria to the nucleus, which are involved in the stimulation of mitochondrial growth. Notably, the molecular mechanism regulating the biogenesis of mitochondrial lipids is poorly understood.

In this study, we identified factors whose expression was enhanced by depletion of mtDNA. One of them was found to increase total mitochondrial mass without a pathogenic swelling, when overexpressed. Thus, the factor is involved in the accumulation of mitochondria in response to mitochondrial dysfunction.

## Materials and Methods

### Cells and culture

EB8 and Ft2-11 were described previously (Hayashi et al., 1991; Hayashi et al., 1994). EB8 is a clone, derived from HeLa cells, completely lacking mtDNA, whereas Ft2-11 was constructed by transferring wild-type mtDNA into EB8 so that Ft-2-11 has the same nucleus as EB8. Stable transfectants expressing MIDAS constitutively were constructed from HeLa cells by transfection with *MIDAS* cDNA under the control of the CMV promoter or its empty vector (pCMV-SPORT; Life Technologies).

Stable transfectants expressing siRNA of *MIDAS* were constructed from HeLa cells by transfection with the pSilencer vector (Ambion) with inserts targeting *MIDAS* (5′-AAGCTTTTCCAAAAAAGTGG-AATGTCTGAAGGCCATCTCTTGAATGGCCTTCAGACATTCC-ACGGGATCC-3′) or a random sequence.

HeLa cells and stable transfectants were cultured in DMEM/F-12 (1:1) (Gibco-BRL) supplemented with 10% FBS and 1% penicillin/streptomycin (Gibco-BRL).

### Construction of Myc-tagged MIDAS

To insert the Myc tag at the N-terminus of MIDAS, an *Eco*RI site was generated at the 5′ end of the *MIDAS* coding sequence by PCR and was cloned into the pCMV-SPORT vector. An oligonucleotide encoding MEQKLISEEDLNS (Myc tag sequence underlined) was inserted at the newly generated *Eco*RI site of *MIDAS*. To construct the Myc tag at the C-terminus of MIDAS, a *Bam*HI site was generated at the 3′ end of the coding sequence and an oligonucleotide encoding DPEQKLISEEDL was inserted.

### Differential display

Poly(A)$^+$ RNA was purified from Ft2-11 and EB8 and reverse transcribed. Resultant cDNAs were amplified using arbitrary primer sets, followed by 5% PAGE. The gel was stained with Vistra Green (Amersham Biosciences) and visualized with a Fluoro Imager (Molecular Dynamics) (Liang and Pardee, 1992).

### Antibodies

Anti-MIDAS polyclonal rabbit antiserum was raised against His-tagged MIDAS expressed in *Escherichia coli*. Anti-MIDAS antibody was affinity purified by binding to the MIDAS protein isolated by SDS-PAGE, followed by transfer onto a PVDF membrane. Anti-Tom20 and anti-Tom40 were gifts from K. Mihara, Kyushu University, Japan. Other antibodies were purchased as follows: anti-actin (clone AC-40) and anti-β-tubulin from Sigma; anti-p230 antibody and anti-Syntaxin6 from BD Biosciences; anti-Hsc70 antibody from Santa Cruz; anti-Hsp60 from MBL; anti-cytochrome c antibody and anti-Cox4 from Clontech; and anti-SDH70, anti-SDH30, anti-COX I and anti-COX II antibodies from Molecular Probes.

### Immunohistochemical staining of muscle sections

Biopsy samples were obtained from the biceps brachii muscle with informed consent and then frozen in isopentane and liquid nitrogen. Frozen sections 6 μm thick were stained histochemically and immunologically. Activities of SDH and COX were visualized as described previously (Hasegawa et al., 1991; Dubowitz, 1985). The expression of MIDAS was detected with anti-MIDAS antibody. The polyclonal antibody against MIDAS was diluted 500-fold with 10% BSA in PBS and incubated with sections for 5 hours at 37°C and then MIDAS was detected with DAB using an indirect streptavidin-biotin immunohistochemical method, according to the manufacturer's protocol (Histofine, Nichirei, Co. Ltd., Tokyo, Japan). The MIDAS protein expressed was semi-quantified by the density of staining.

### Immunocytostaining of cultured cells

Cultured cells were fixed with 4% paraformaldehyde in PBS for 20 minutes at room temperature. After a wash with PBS, they were treated with 5% acetic acid in ethanol for 10 minutes at –20°C to permeabilize membranes, then incubated in a blocking buffer (3% BSA and 3% goat serum in PBS) and overnight at 4°C in the blocking buffer containing primary antibody. After another wash with PBS, the cells were incubated in the blocking buffer containing labeled secondary antibody and visualized with a confocal laser-scanning microscope (Fluoview FV300, Olympus, Tokyo, Japan). As an alternative, we used another method described (Bell et al., 2001). In brief, cells were fixed for 10 minutes with 4% paraformaldehyde and 4% sucrose without treatment for permeabilization and incubated with primary antibody, followed by secondary antibody.

### Subfractionation of HeLa cells

Cells were homogenized as described (Trounce et al., 1996). The homogenate was applied to a 7-35% (w/v) Nycodenz preformed continuous density gradient and centrifuged in a swinging-bucket rotor at 77,000 $g_{AV}$ for 4 hours. The fractions were collected from the top of the gradient. The MIDAS protein was semi-quantified by the density of total bands in western blots. The sub-organellar fractionation of mitochondria (fraction number 15) was performed as described (Kanamori et al., 2003).

### Electron microscopy

Cells were cultured on plastic dishes and fixed with 2% glutaraldehyde in PBS. Ultra-thin sections were stained with uranyl acetate and lead nitrate and examined with an H-7000 electron microscope (Hitachi, Tokyo, Japan).

### Flow cytometry

Living transfectants were stained with 20 nM MitoTracker Red CMXRos (Molecular Probes) or 100 nM MitoTracker Green (Molecular Probes) for 30 minutes at 37°C, treated with trypsin and subjected to a flow cytometric analysis with an Epics Elite ESP (Coulter).

### Three-dimensional imaging

Living cells were stained with 20 nM MitoTracker Red and 500 nM SYTO 16 (Molecular Probes) for 30 minutes at 37°C. The cells were scanned using 0.4 μm sections with the confocal laser-scanning microscope. Three-dimensional (3D) views were reconstructed with Fluoview software (Olympus) and volumes of the nucleus and mitochondria were calculated by summing fluorescent areas from each section using the NIH Image program (developed at the US National Institutes of Health and available on http://rsb.info.nih.gov./nih-image).

### Separation of phospholipids

Total lipids were extracted from transfectants using methanol/chloroform as described (Folch et al., 1957). For the separation and detection of phospholipids, total lipids were injected into a HPLC system (model 616; Waters) fitted with a Wakosil 5Sil column (Wako, Tokyo, Japan). The mobile phase was a mixture of n-hexan, isopropanol, ethanol, acetic acid and 25 mM potassium phosphate buffer (pH 7.0) (146:282.5:50:0.3:31; v/v/v/v/v). The flow rate was 1 ml/minute. The elution of phospholipids was monitored at 205 nm with the UV detector (SPD-10A; Shimadzu). Retention times and quantities of phospholipids were determined using a phospholipid kit (Doosan Serdary Research Laboratory) as a standard.

## Results

### Cloning of genes that respond to a depletion of mtDNA

To identify nuclear genes that respond to a depletion of mtDNA, we screened for mRNA whose expression increased in cells lacking mtDNA using the differential mRNA display technique (Liang and Pardee, 1992) (Fig. 1A) by comparing mRNA populations in a HeLa derivative lacking mtDNA (EB8) (Hayashi et al., 1991) and control cybrid cells (Ft2-11) (Hayashi et al., 1994). Bands 1 and 2, which were stronger in EB8 than in Ft2-11 (Fig. 1A), were found to correspond to the apurinic/apyrimidinic endonuclease I (APE1/HAP1) (Demple et al., 1991) and DNA ligase III genes (Wei et al., 1995), respectively. The products of these genes are localized in mitochondria and involved in mtDNA repair (Kang and Hamasaki, 2002).

DNA sequencing distinguished the gene corresponding to the third band in Fig. 1A from the genes which have been so far identified to be involved in mitochondrial biogenesis, gene expression and metabolism. The full-length cDNA was isolated from a human brain cDNA library (Gibco-BRL) to confirm the increase in its mRNA (Fig. 1B,C) and its product (Fig. 1D,E) by northern and western blotting, respectively. We named this gene *MIDAS* (mitochondrial DNA absence sensitive factor), because the gene product was expressed in response to mtDNA depletion. Interestingly, the nucleotide sequence was identical to *GPP34* (GenBank accession no. AJ296152) whose product has been identified as a Golgi protein of unknown function(s) (Bell et al., 2001). In addition, MIDAS/GPP34 contains an isoform named GPP34R (GenBank accession no. AJ296153), which is highly homologous with MIDAS/GPP34 (supplementary material Fig. S1). In fact, GPP34R was expressed in cells with the HeLa nucleus as detected by northern blotting (supplementary material Fig. S2A). Interestingly, GPP34R was also expressed more abundantly in EB8 than in Ft2-11 (supplementary material Fig. S2A). The relative amount of GPP34R mRNA was semi-quantified by the TaqMan probe method and found to be less than 2% of that in

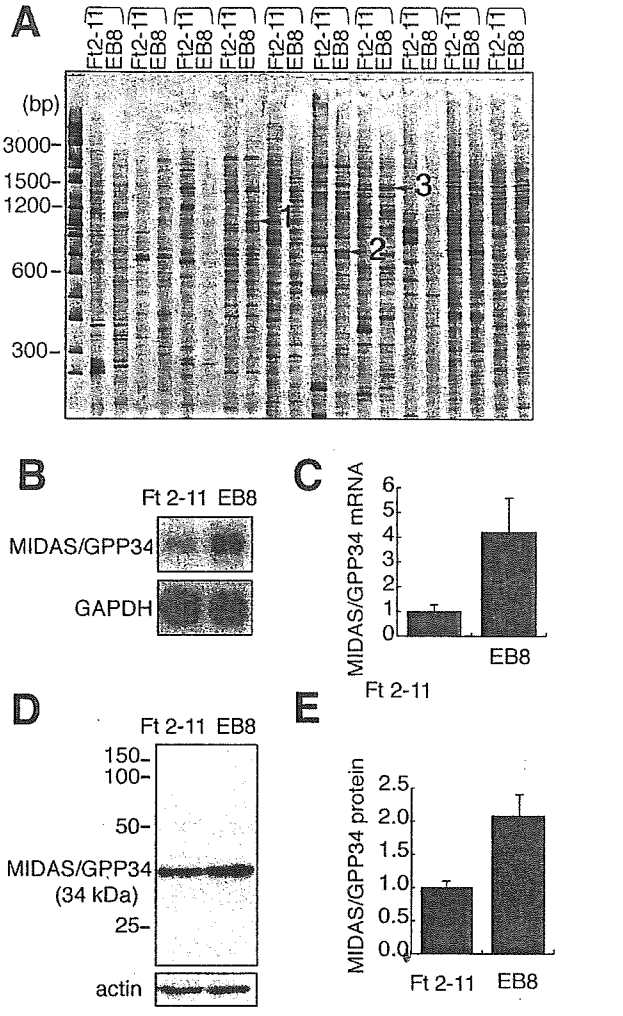


**Fig. 1.** Enhanced expression of MIDAS/GPP34 in EB8 (mtDNA-free HeLa cells). (A) Comparison of mRNA obtained from Ft2-11 with that from EB8 by differential display. EB8 lacks mtDNA whereas Ft2-11 is derived from EB8 but has wild-type mitochondria. Ten sets of arbitrarily primed PCR products were subjected to 5% PAGE. Three bands indicated by arrows were cloned and sequenced. Bands 1, 2 and 3 corresponded to apurinic/apyrimidinic endonuclease I, DNA ligase III and MIDAS/GPP34, respectively. (B) Northern blots of total RNA extracted from Ft2-11 and EB8 were hybridized with *GPP34*- and *GAPDH* (glyceraldehyde-3-phosphate dehydrogenase)-specific probes. (C) *GPP34* mRNA levels normalized to *GAPDH* levels based on the mean values±s.d. for three sets of northern blotting experiments (vertical bars). (D) Western blotting of Ft2-11 and EB8. Whole-cell lysates were separated by 12% SDS-PAGE and transferred onto a PVDF membrane. MIDAS/GPP34 was immunostained with anti-MIDAS antibody. (E) The MIDAS/GPP34 protein normalized against actin. Mean values of three sets of experiments are shown with s.d. (vertical bars).

MIDAS/GPP34 (supplementary material Fig. S2B). Therefore, we focused on the function of MIDAS/GPP34.

### Specific expression of MIDAS/GPP34 in muscle fibers with abnormal mitochondria

Mitochondria accumulate in response to their own dysfunction

in mitochondrial diseases (Schon, 2000; Wallace, 1999). We examined the expression of MIDAS/GPP34 in muscle fibers of patients with mitochondrial diseases. Large deletions and a point mutation in the $tRNA^{Leu(UUR)}$ gene of mtDNA are responsible for the subgroups of mitochondrial diseases, CPEO (chronic progressive external ophthalmopelia) (Holt et al., 1988; Shoubridge et al., 1990) and MELAS (mitochondrial myopathy, encephalopathy, lactic acidosis and stroke-like episodes) (Goto et al., 1990; Kobayashi et al., 1990; Kobayashi et al., 1991), respectively. Accumulations of abnormal mitochondria are detected as ragged-red fibers and high succinate dehydrogenase (SDH) fibers, with mutant mtDNA dominating in a mosaic manner (Engel and Cunningham, 1963; Hasegawa et al., 1991; Lightowlers et al., 1997).

Muscle sections from a normal subject and patients with CPEO or MELAS were stained for activity of SDH and cytochrome c oxidase (COX) and with anti-MIDAS antibody. No MIDAS-positive fibers were detected in normal muscle, whereas MIDAS-positive fibers were detected in the muscle sections of affected patients (Fig. 2). The amount of MIDAS in the positive muscles increased approximately twofold compared to those in the negative muscles. It is noted that MIDAS was more abundant specifically in fibers with an $SDH^{++}/COX^{-}$ phenotype (Fig. 2, asterisks). Thus, MIDAS is expressed in response to mitochondrial dysfunction in muscle with mitochondrial diseases.

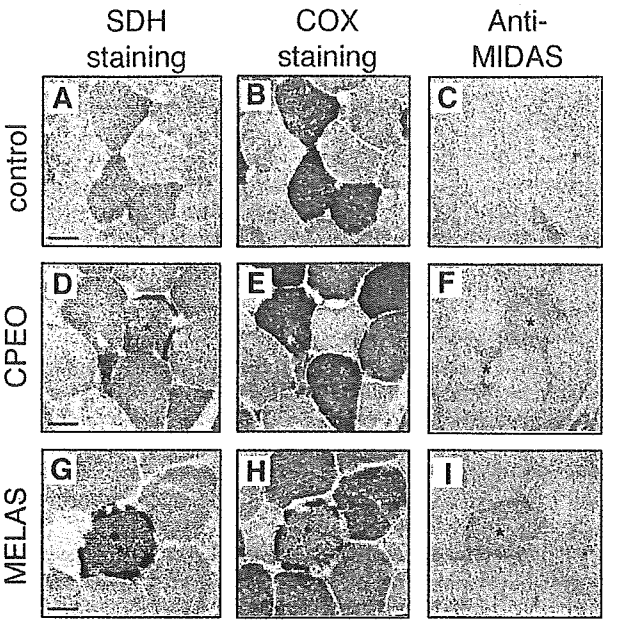


**Fig. 2.** Expression of MIDAS/GPP34 in $SDH^{++}/COX^{-}$ muscle cells of patients with mitochondrial diseases. Biopsy samples were obtained from the biceps brachii muscle. Activities of SDH and COX were visualized histochemically and the expression of MIDAS/GPP34 was detected with anti-MIDAS antibody. (A-C) Control muscle without mitochondrial disorder. (D-F) Muscle from a patient with CPEO who has a common deletion in mtDNA. (G-I) Muscle from a patient with MELAS who has a point mutation at nucleotide number 3243 in the $tRNA^{Leu(UUR)}$ gene. Asterisks indicate $SDH^{++}/COX^{-}$ cells of patients with increased MIDAS/GPP34 expression. Bars, 50 μm.

## Subcellular distribution of MIDAS/GPP34

GPP34 has been isolated as a Golgi peripheral membrane protein in a Golgi proteomics study (Bell et al., 2001). To verify the distribution of MIDAS in mitochondria, we immunostained HeLa cells with an affinity-purified polyclonal antibody against the MIDAS protein. Immunostaining of HeLa cells revealed that MIDAS mainly colocalized with MitoTracker Red (Fig. 3A). The mitochondrial localization was confirmed with another mitochondrial marker, Hsp60 (data not shown). With careful observation, we found MIDAS in an additional region, the perinuclear area, where MitoTracker Red was absent (Fig. 3A, merge; indicated by white arrowhead). This region corresponds to the Golgi apparatus, as judged by immunostaining with anti-p230 (the *trans*-Golgi membrane protein) (Erlich et al., 1996) antibody (Fig. 3B). These results suggest that a majority of MIDAS/GPP34 localizes to mitochondria, but some is distributed in the Golgi apparatus.

This finding disagrees with the previous study on GPP34 showing that GPP34 is located in the Golgi apparatus, but not in mitochondria (Bell et al., 2001). This discrepancy could be due to a different fixation method prior to staining. In general, for immunostaining of cultured cells, the permeabilization of intramembranes with an organic solvent or detergent is essential for antibodies to penetrate the membranes of organelles (Zeller, 1998). In fact, under the same conditions as the published experiment (no permeabilization pretreatment), MIDAS did not show colocalization with mitochondria (Fig. 3D), being detected only in the Golgi apparatus (Fig. 3E). Moreover, several marker proteins were immunostained to confirm that the permeabilization pretreatment with acetate in cold ethanol is essential for detecting the mitochondrial proteins located internally. Without permeabilization pretreatment, cytosolic (Hsc70), mitochondrial outer membrane (Tom20) and *trans*-Golgi (p230) proteins were stained with each antibody (Fig. 3F), whereas the mitochondrial intermembrane space protein (cytochrome c) could not be detected (Fig. 3F). Alternatively, cytochrome c required an acetate/ethanol pretreatment for permeabilization as described in Materials and Methods to be detected (Fig. 3C). Moreover, a mitochondrial matrix protein (Hsp60) and an inner membrane protein (SDH70) were clearly stained only with the acetate/ethanol pretreatment (supplementary material Fig. S3). Therefore, the mitochondrial MIDAS/GPP34 protein is located inside mitochondria or embedded in the outer membrane. In addition, immunostaining with anti-KDEL, the signal peptide targeting the endoplasmic reticulum (ER) (Munro and Pelham, 1987), showed no localization of MIDAS/GPP34 to the ER (data not shown).

To further investigate the subcellular distribution of MIDAS, Myc-tagged constructs were generated. A gene corresponding to a Myc peptide was fused to the gene of the N-terminus (Myc-MIDAS) or C-terminus (MIDAS-Myc) of MIDAS. Fusion constructs were transfected into HeLa cells and the cells were allowed to express the protein for 16 hours. The transfected cells were immunostained with anti-Myc antibody. Myc-MIDAS was localized to the perinuclear area and colocalized with the p230 *trans*-Golgi (Fig. 3G). On the other hand, MIDAS-Myc was distributed in both mitochondria and Golgi as stained with anti-MIDAS antibody (Fig. 3H). This

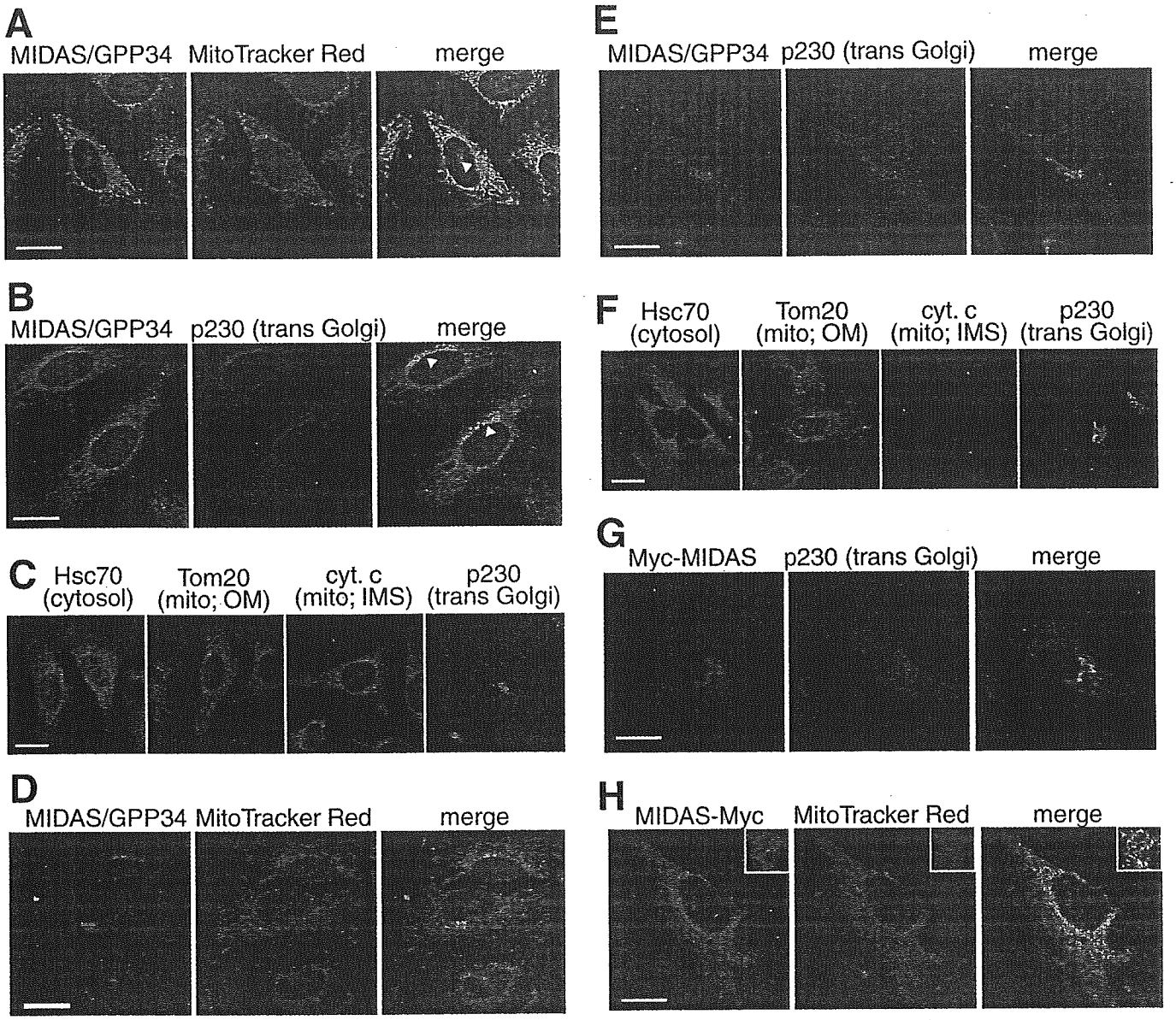


**Fig. 3.** Localization of MIDAS/GPP34 in mitochondria and the Golgi apparatus. (A-C) HeLa cells in culture were fixed, permeabilized with 5% acetic acid in ethanol and then immunostained with various antibodies. (A) MitoTracker Red (100 nM) was added as a mitochondrial indicator prior to fixation. MIDAS/GPP34 was detected with anti-MIDAS antibody. Arrowhead indicates where MIDAS/GPP34 is more abundant than mitochondria in a perinuclear area. (B) MIDAS/GPP34 and p230 (*trans*-Golgi) were double-stained immunochemically using different secondary antibodies. Arrowheads indicate where the perinuclear area was co-stained with both antibodies. (C) Hsc70 (cytosol), Tom20 (outer membrane of mitochondria), cytochrome c (cyt. c) (intermembrane space of mitochondria) and p230 (*trans*-Golgi) were detected with their respective antibodies. (D-F) HeLa cells in culture were fixed with 4% paraformaldehyde and 4% sucrose without treatment for permeabilization and immunostained with the same procedure as in (A-C). (G,H) Localization of Myc-tagged MIDAS. A Myc tag was fused to the N-terminus (G) or C-terminus (H) of MIDAS. Fusion constructs were transfected into HeLa cells and cells were allowed to express protein for 16 hours. Cells were stained with anti-Myc, anti-p230 antibodies or MitoTracker Red with the same procedure as in (A-C). Bars, 20 μm.

finding suggests that MIDAS potentially localizes to both mitochondria and the Golgi apparatus.

To demonstrate the subcellular distribution of MIDAS, organelles were sub-fractionated with a Nycodenz gradient. HeLa cells were homogenized, the homogenate was fractionated with a 7-35% density gradient and the distribution of MIDAS was examined by western blotting (Fig. 4A). The majority of MIDAS was detected in the mitochondrial fractions (with Tom20 and Hsp60) and small portions were fractionated with the Golgi (with a Golgi marker, Syntaxin6) and cytosol. Relative amounts of MIDAS distributed in the fractions for mitochondria (fractions 13-17), Golgi (fractions 6-12) and cytosol (fractions 1-5) were 0.75, 0.19 and 0.06, respectively, as judged by the densities of total bands.

To determine the sub-mitochondrial distribution of MIDAS, the mitochondria purified from HeLa cells were treated with

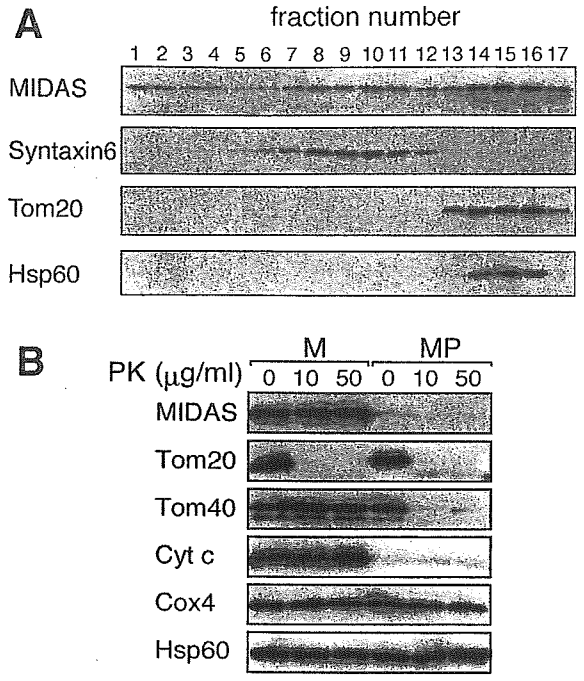


**Fig. 4.** Localization of MIDAS/GPP34 in the mitochondrial intermembrane space. (A) Fractionation of organelles of HeLa cells in 7-35% (w/v) preformed density gradients. The distribution of MIDAS was detected by western blotting. Syntaxin6 was used for a Golgi marker. Tom20 and Hsp60 were used for mitochondrial markers. (B) Mitoplasts were obtained from the mitochondrial fraction (fraction 15 in A) by osmotic disruption of the outer membrane. The mitochondria (M; lanes 1-3) and the mitoplasts (MP; lanes 4-6) were treated with proteinase K (PK; 10 μg/ml or 50 μg/ml). Mitochondrial sub-fractions were monitored by western blotting with antibodies directed against Tom20 (an outer membrane protein; most of which is exposed outside mitochondria), Tom40 (an outer membrane protein), cytochrome c (cyt c) (an intermembrane space protein), Cox4 (an inner membrane protein) and Hsp60 (a matrix space protein).

proteinase K. Both Tom40 and Tom20 are embedded in the outer membrane, whereas Tom20 is exposed to the outside of mitochondria (Pfanner and Geissler, 2001). Tom20 was easily digested with 10 μg/ml proteinase K, whereas Tom40 and MIDAS were resistant (Fig. 4B, M). On the other hand, when mitochondria were converted to mitoplasts, MIDAS disappeared (Fig. 4B, MP) even without proteinase K, as cytochrome c disappeared. From these results, it was concluded that the majority of MIDAS protein is located in the intermembrane space of mitochondria, with a small fraction present in the Golgi apparatus.

## Mitochondrial accumulation without swelling by MIDAS

To determine the function of MIDAS in mitochondria, HeLa cells were transfected with *MIDAS* cDNA under the control of the CMV promoter. We could isolate transfectants constitutively expressing MIDAS at low levels (1.5- to 2-fold increase) (Fig. 5A, upper left panel, CMV-MIDAS3 and CMV-MIDAS9). Cells transiently transfected with a higher level of MIDAS could undergo cell division once or twice but did not survive for a week (data not shown), suggesting that overproduction of MIDAS prevents cell growth. To downregulate MIDAS, we then constructed HeLa transfectants expressing siRNA (small interfering RNA) of *MIDAS* to inhibit the endogenous MIDAS expression (Fig. 5A, upper right panel).

These transfectants were stained with MitoTracker Red to visualize mitochondria, in a short period to monitor the membrane potential of mitochondria. Even low levels of additional MIDAS expression caused a change in the distribution of mitochondria. The mitochondria in a *MIDAS* transfectant CMV-MIDAS3 were concentrated around the nucleus (Fig. 5B, second panel), whereas those in the control transfectants remained dispersed (Fig. 5B, first panel).

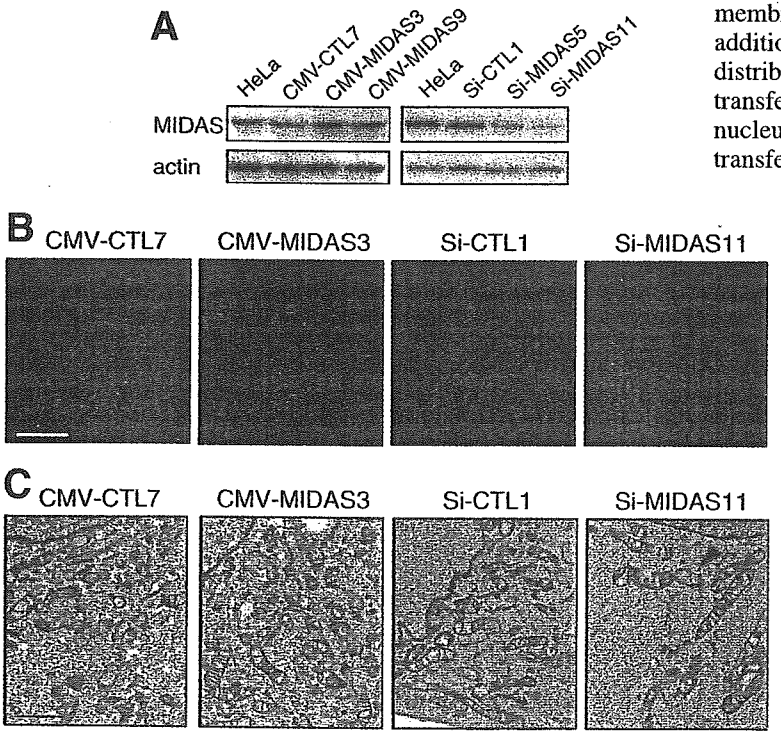


**Fig. 5.** The increased or decreased mass of intact mitochondria related to MIDAS concentration. (A) CMV-CTL7 and Si-CTL1 are stable control transfectants derived from HeLa cells. Although CMV-MIDAS3 and CMV-MIDAS9 are stable *MIDAS* transfectants under the control of the CMV promoter. Si-MIDAS5 and Si-MIDAS11 were transfectants expressing siRNA of *MIDAS* constitutively. Total cell lysate was extracted from each transfectant cell line and subjected to western blotting with anti-MIDAS and anti-actin antibodies. (B) Control (CMV-CTL7 and Si-CTL1), *MIDAS* transfectants (CMV-MIDAS3) and siRNA *MIDAS* transfectants (Si-MIDAS11) were stained with MitoTracker Red and visualized by confocal scanning laser microscopy. (C) Electron micrographs (×8000) of mitochondria in the transfectants. Bar, 20 μm (B); 1 μm (C).